

**A THEORETICAL STRUCTURAL IMPAIRMENT DETECTION SYSTEM FOR
TIMBER RAILWAY BRIDGES**

A Thesis

by

JOHN PAUL ORSAK

Submitted to the Office of Graduate Studies of
Texas A&M University
in partial fulfillment of the requirements for the degree of

MASTER OF SCIENCE

May 2012

Major Subject: Civil Engineering

A Theoretical Structural Impairment Detection System for Timber Railway Bridges

Copyright 2012 John Paul Orsak

**A THEORETICAL STRUCTURAL IMPAIRMENT DETECTION SYSTEM FOR
TIMBER RAILWAY BRIDGES**

A Thesis

by

JOHN PAUL ORSAK

Submitted to the Office of Graduate Studies of
Texas A&M University
in partial fulfillment of the requirements for the degree of

MASTER OF SCIENCE

Approved by:

Chair of Committee,	Gary Fry
Committee Members,	Harry Jones
	Alan Palazzolo
Head of Department,	John Niedzwecki

May 2012

Major Subject: Civil Engineering

ABSTRACT

A Theoretical Structural Impairment Detection System for Timber Railway Bridges.

(May 2012)

John Paul Orsak, B.S., Texas A&M University

Chair of Advisory Committee: Dr. Gary Fry

The objective of this research is to develop a theoretical Structural Impairment Detection System (SIDS) for timber railway bridges. Due to fatigue, the timber stringers in timber railway bridges develop shear cracks. These shear cracks lead to higher bridge deflections, higher stresses in the stringers and rail, and shorter fatigue life of the system. A SIDS is proposed which links wheel path accelerations obtained from traversing freight cars to the condition of the bridge.

In order to develop the SIDS, two models of timber railway bridges with various levels of structural impairment were developed. The first model was a quasi-static model developed from classical beam theory and implemented in MATLAB. The second model was a dynamic, finite element model created in LS-DYNA. Traversing axle loads were imposed on the models. The results obtained from the model were the wheel paths the axles take as they traverse the bridge. The paths were expressed as vertical displacements as a function of position on the bridge. Wheel path accelerations were obtained by numerically differentiating the vertical displacements.

The accelerations were then used to train neural networks to have an input of an acceleration vector and an output of a bridge condition vector. The neural networks were trained on results from both models under three train speeds: 40 mph, 30 mph, and 20 mph. The networks were able to determine the correct bridge condition 90% of the time

when the train speed was 40 mph and 70% of the time when the train speed was 30 mph. The networks were not successful in determining bridge condition when the train speed was 20 mph.

DEDICATION

To my family

ACKNOWLEDGEMENTS

I would like to thank my committee chair, Dr. Gary Fry, and my committee members, Dr. Harry Jones and Dr. Alan Palazzolo for their guidance and support throughout the course of this research. Furthermore, I would like to thank the senior members of my research group for mentorship and encouragement. Finally, I thank my mother and father for always believing in me.

TABLE OF CONTENTS

	Page
ABSTRACT	iii
DEDICATION	v
ACKNOWLEDGEMENTS	vi
TABLE OF CONTENTS	vii
LIST OF FIGURES.....	x
LIST OF TABLES	xiii
NOMENCLATURE.....	xiv
 CHAPTER	
I INTRODUCTION AND BACKGROUND.....	1
1.1 Introduction	1
1.2 Objective	1
1.3 Timber Bridge Background.....	1
1.4 Neural Network Background	3
1.5 Crack Development in Timber Stringers.....	4
1.6 Theoretical Stress Effect of Crack	4
1.7 Previous Testing of Timber Stringers	5
II MODELING PROCEDURES.....	6
2.1 Overview of Modeling	6
2.2 Model and Load Parameters.....	6
2.3 Analytical Model.....	7
2.4 LS-DYNA Model.....	11
2.5 Model Comparison.....	13
2.6 MATLAB and LS-DYNA Analysis Cases	14

CHAPTER	Page
III	MODELING RESULTS 15
	3.1 Results from MATLAB Model 15
	3.2 Results from LS-DYNA Model 16
IV	NEURAL NETWORK DEVELOPMENT 18
	4.1 Overview of Neural Network Development 18
	4.2 Network Architecture 18
	4.3 Creating Training and Testing Vectors 19
	4.4 Training and Testing the Networks 20
	4.5 Agreement Criterion for Determining Bridge Condition 20
V	NEURAL NETWORK RESULTS 22
	5.1 Explanation of Table Structure 22
	5.2 Networks from 20 MPH Train Speed Cases 22
	5.3 MATLAB Acceleration Input Networks 23
	5.4 LS-DYNA Acceleration Input Networks 23
	5.5 Combined Acceleration Input Networks 23
VI	DISCUSSION 24
	6.1 Displacements and Accelerations from MATLAB Model 24
	6.2 Displacements and Accelerations from LS-DYNA Model 25
	6.3 20 MPH Train Speed Networks 26
	6.4 The Effect of Load Magnitude on Accelerations 26
	6.5 General Network Performance 27
VII	CONCLUSIONS 29
	7.1 Conclusions 29
	7.2 Future Research 29

	Page
REFERENCES	31
APPENDIX A FIGURES.....	33
APPENDIX B TABLES	60
APPENDIX C CODE FOR MATLAB MODEL.....	63
VITA	65

LIST OF FIGURES

FIGURE	Page
1.1 Typical cross section of a timber railroad bridge.....	33
1.2 Example of a multi-layer perceptron.....	33
1.3 Timber stringer with typical horizontal shear crack.....	34
1.4 Stress distribution of intact beam.....	34
1.5 Stress distribution in a cracked beam.....	35
2.1 Freight car connection load.....	35
2.2 Two-span beam representing a timber railway bridge.....	36
2.3 Bridge model consisting of a rail beam and a stringer beam.....	36
2.4 Four axle loads traversing two-span bridge.....	36
2.5 Overall view of the LS-DYNA model.....	37
2.6 Close-up view of one half of the LS-DYNA model.....	37
2.7 Point masses controlled by ramp functions.....	38
2.8 Comparison of models – 1 st wheel path.....	38
2.9 Effect of extended rails (ER) and self-weight (SW).....	39
2.10 Observation points.....	39
3.1 Path 1 MATLAB wheel path displacements.....	40
3.2 Path 2 MATLAB wheel path displacements.....	40
3.3 Path 3 MATLAB wheel path displacements.....	41
3.4 Path 3 MATLAB wheel path displacements.....	41

3.5	Path 1 MATLAB wheel path accelerations – 40 mph	42
3.6	Path 2 MATLAB wheel path accelerations – 40 mph	42
3.7	Path 3 MATLAB wheel path accelerations – 40 mph	43
3.8	Path 4 MATLAB wheel path accelerations – 40 mph	43
3.9	Path 1 LS-DYNA wheel path displacements – 40 mph	44
3.10	Path 2 LS-DYNA wheel path displacements – 40 mph	44
3.11	Path 3 LS-DYNA wheel path displacements – 40 mph	45
3.12	Path 4 LS-DYNA wheel path displacements – 40 mph	45
3.13	Path 1 LS-DYNA wheel path accelerations – 40 mph	46
3.14	Path 2 LS-DYNA wheel path accelerations – 40 mph	46
3.15	Path 3 LS-DYNA wheel path accelerations – 40 mph	47
3.16	Path 4 LS-DYNA wheel path accelerations – 40 mph	47
3.17	Path 1 LS-DYNA wheel path displacements – 30 mph	48
3.18	Path 2 LS-DYNA wheel path displacements – 30 mph	48
3.19	Path 3 LS-DYNA wheel path displacements – 30 mph	49
3.20	Path 4 LS-DYNA wheel path displacements – 30 mph	49
3.21	Path 1 LS-DYNA wheel path accelerations – 30 mph	50
3.22	Path 2 LS-DYNA wheel path accelerations – 30 mph	50
3.23	Path 3 LS-DYNA wheel path accelerations – 30 mph	51
3.24	Path 4 LS-DYNA wheel path accelerations – 30 mph	51
3.25	Path 1 LS-DYNA wheel path displacements – 20 mph	52
3.26	Path 2 LS-DYNA wheel path displacements – 20 mph	52

3.27	Path 3 LS-DYNA wheel path displacements – 20 mph	53
3.28	Path 4 LS-DYNA wheel path displacements – 20 mph	53
3.29	Path 1 LS-DYNA wheel path accelerations – 20 mph.....	54
3.30	Path 2 LS-DYNA wheel path accelerations – 20 mph.....	54
3.31	Path 3 LS-DYNA wheel path accelerations – 20 mph.....	55
3.32	Path 4 LS-DYNA wheel path accelerations – 20 mph.....	55
4.1	Network architecture	56
4.2	Output vector options	56
4.3	Logsig function	57
4.4	Acceleration vector with noise added	57
6.1	Comparison between displacements from MATLAB and LS-DYNA path 2	58
6.2	Comparisons between accelerations from MATLAB and LS-DYNA path 2	58
6.3	Comparisons between accelerations at different train speeds.....	59
6.4	Path 4 LS-DYNA wheel path accelerations – 20 mph.....	59

LIST OF TABLES

TABLE	Page
1.1 Summary of previous testing.....	60
2.1 General bridge parameters	60
2.2 Material properties	60
5.1 Percentage of correct outputs – MATLAB input, 40 mph train speed	61
5.2 Percentage of correct outputs – MATLAB input, 30 mph train speed	61
5.3 Percentage of correct outputs – LS-DYNA input, 40 mph train speed.....	61
5.4 Percentage of correct outputs – LS-DYNA input, 30 mph train speed.....	62
5.5 Percentage of correct outputs – combined input, 40 mph train speed.....	62
5.6 Percentage of correct outputs – combined input, 30 mph train speed.....	62

NOMENCLATURE

a	acceleration
c	distance from neutral axis to extreme fiber of beam
D	damping coefficient
DAF	dynamic amplification factor
EI	flexural rigidity of a beam
F_d	damping force
I	moment of inertia about neutral axis
L	length
m	mass
M	bending moment
M_0	initial bending moment
P	total applied vertical load
P_r	load carried by rail
P_s	load carried by stringer
R_b	support reaction force
v	velocity
V	shear force
V_0	initial shear force
SIDS	structural impairment detection system
w	deflection

w_0	initial deflection
δ	total deflection of rail/stringer bridge beam
δ_r	rail deflection
δ_s	stringer deflection
ξ	distance from left support to point load
σ	normal stress under bending
θ_0	initial angle of rotation

CHAPTER I

INTRODUCTION AND BACKGROUND

1.1 Introduction

Timber bridges make up a significant portion of current railroad bridges. As a general rule, these aging timber bridges require frequent inspection and maintenance operations systems exhibit inferior performance when compared to modern concrete or steel short-span systems. Current damage detection techniques predominantly involve manual inspections performed by experienced technicians. In the past twenty years, extensive research has been conducted in the area of using electric sensors (e.g. strain gauges, accelerometers, etc.) as a means to enhance manual inspections. Much of this research focuses on a bridge by bridge approach involving a separate experimental setup for each bridge of interest. Due to the number of timber bridges in service, this approach is exceedingly costly and time-consuming.

1.2 Objective

The goal of this research is to develop a theoretical Structural Impairment Detection System (SIDS) to determine the structural fitness of any timber railroad bridge with traffic. In order to accomplish this, a timber bridge loaded by a freight car will be modeled both quasi-statically and dynamically. Vertical accelerations of the freight car will be extracted from the models. These accelerations will then be fed into a neural network. The output of the neural network will be a vector correlating to the structural fitness of the bridge. The overall goal is to develop a proof of concept of how such a SIDS would work.

1.3 Timber Railroad Bridge Background

Even though repairs and reconstructions have occurred, many timber bridges have been continually in service for over 100 years (Peterson and Gutkowski 1997). Across the

This thesis follows the style of *Journal of Structural Engineering*.

United States, timber bridges account for 20% of railroad bridges in northern states and up to 40% in some southern states (Radford et al. 2002). A typical cross section of such bridges is presented in Figure 1.1. The axle load travels from the rail, to the cross ties, to two chords of longitudinal stringers, to the piles, and finally to the soil. The extent to which the piles penetrate into the ground is not shown in Figure 1.1.

Continuous use and years of decay have rendered 47% of timber bridges “structurally deficient” by the National Bridge Inventory (Radford et al. 2002). This designation is based upon visual inspection for defects. In addition to the aging status of the timber railroad bridge infrastructure, railcar axle loads are increasing from 37.5 tons up to 39 tons to increase capacity and efficiency (Peterson and Gutkowski 1997). These axle load increases warrant even closer scrutiny in monitoring existing bridges.

Advanced timber bridge inspection techniques have been investigated in the past in order to better evaluate timber bridges. Peterson and Gutkowski (1997) used a combined dynamic and ultrasonic technique to evaluate the structural integrity of timber bridges. Emerson, et al. (1998) summarized different non-destructive evaluation techniques for timber. These techniques include visual inspection, stress waves, ultrasonic inspection (i.e. high frequency stress waves), drill resistance, radiography, microwave, and vibration. Morison et al. (2002) used impact hammers to generate frequency response functions in order to determine if decay damage was present in timber bridges. Moreu and Nagayama (2008) used wireless sensors to measure the acceleration of timber trestle railroad bridges.

What these papers and other research efforts have in common is that they focus on the direct evaluation of the bridge structure itself. By necessity, this leads to a bridge by bridge method in which a separate sensor array or evaluation technique must be installed or employed on each bridge. With thousands of timber bridges still being used in the United States (Federal Highway Administration 2009), the amount of manpower and

money necessary to provide these sorts of advanced evaluations is much greater than visual evaluations alone. Thus, a SIDS which could easily and rapidly be applied to multiple bridges would be a valuable asset.

1.4 Neural Networks Background

Neural networks will be utilized to link vertical accelerations of the railcar to structural fitness. Originally conceived by Rosenblatt (1958), a neural network is a system of functional nodes, called neurons, designed to emulate the learning abilities of a brain (Hagan 1996). An example neural network schematic is shown in Figure 1.2.

Specifically, this type of neural network is called a multi-layer perceptron. An input vector, X , is entered into the network and multiplied by a set of weights. Each vector input is multiplied by a separate weight and then collected at the beginning of the first hidden layer. The collected values are added together and then fed into the hidden layer neuron. The hidden layer neurons pass the inputs through transfer functions, represented by F_n . The transfer functions are typically sigmoid or linear functions. The output of the transfer functions is then multiplied by a separate set of weights. Next, the values can be passed through another hidden layer, or they can be outputted in the output layer. There is no limit to the numbers of layers or neurons possible.

In order to train the network, inputs with known outputs are passed through the network. The network outputs are then compared with the known output, and if the error is greater than a pre-specified value, the weights are adjusted. The algorithm repeats until the error is acceptable. This training scheme is referred to as back propagation.

Neural networks have been utilized in previous research efforts involving structural damage identification. Data from instrumented laboratory specimens with known damage states have been fed to neural networks which were able to correctly assess the

damage state (Lee et al. 2004, Li et al. 2006). However, there is still much work to be done in developing a network capable of detecting damage in an actual structure.

1.5 Crack Development in Timber Stringers

One common detrimental impairment to timber railroad bridges is a horizontal shear crack which develops in the stringers. If ignored, this impairment is a precursor to more serious impairment. The crack can develop along nearly the whole length of the stringer and can go through the entire section. Once this crack has developed, the stringer is then referred to as “split”. An in-service stringer with such a crack is shown in Figure 1.3. The crack develops as a result of fatigue and can greatly reduce the structural fitness of the bridge. In addition to further degradation of the bridge, the crack can also lead to degradation in the rail.

1.6 Theoretical Stress Effect of Crack

In order to understand how this shear crack affects structural performance, a review of stresses in beams with rectangular cross-sections is necessary. According to classical beam theory, the maximum stress in a beam with a rectangular cross-section is given by:

$$\sigma = \frac{Mc}{I} \quad (1.1)$$

where σ is the stress, M is the moment, c is the distance from the neutral axis to the top or bottom of the section, and I is the moment of inertia about the neutral axis. The stress distribution is shown in Figure 1.4.

A crack in the beam’s center (i.e. the neutral axis) changes the stresses developed in the beam. If the crack penetrates all the way through the section, the beam can then be considered to be two separate beams, one on top of the other. Half of the moment is carried in each beam, and the c value is half of the previous c value. Each beam has a moment of inertia of $1/8^{\text{th}}$ the value of the original beam. Therefore, the maximum stress in the split beam is:

$$\sigma_c = \frac{(M/2)(c/2)}{(I/8)} = \frac{2Mc}{I} = 2\sigma \quad (1.2)$$

The stress distribution of a split beam is shown below in Figure 1.5.

The split beam is essentially two separate beams each with a moment of inertia equal to $I/8$. Therefore, the total moment of inertia for the beams acting together is the sum of the two beams, equal to $I/4$. Due to the inhomogeneous nature of wood, the flexural behavior of a timber beam is best represented by its flexural rigidity, EI . For the theoretical beam, the modulus of elasticity, E , does not change when the beam is split. Therefore, the theoretical flexural rigidity of a split beam is simply $EI/4$. This is equivalent to a 75% reduction in flexural rigidity.

1.7 Previous Testing of Stringers

Previous testing of intact and split southern pine stringers took place at Texas A&M University from 2000-2002 (Fry et. al. 2003). Two specimens were tested. Both specimens had a cross section measuring 8-inch by 16-inch and a length measuring 15-ft. EI values were calculated from test data before and after the beams were split. The beams were loaded in four-point bending. A summary of the results is shown in Table 1.1.

The average reduction in EI value was 62.6%. Recall the theoretical EI value for a split beam is $1/4^{\text{th}}$ the intact value, or a 75% reduction. The difference comes from the simplicity of the theoretical analysis, which assumes a complete separation and no frictional effects.

CHAPTER II

MODELING PROCEDURES

2.1 Overview of Modeling

Two different models have been developed over the course of the research project. The first is a quasi-static, analytical model derived from Euler Beam Theory and implemented in MATLAB. The second model is a dynamic, LS-DYNA model consisting of finite beam elements and loaded by moving, lumped masses. Neither model takes into account the deformation of the piles, which would result in support deformation.

The goal of the first model is to have complete control over the analysis process by developing an original MATLAB program. The MATLAB model gives an initial understanding of the system and serves as a benchmark for commercial finite element software models. The second model utilizes a fully dynamic, finite element package in order to assess the dynamic response of the system. Both models will be used in the development of the SIDS.

2.2 Model and Load Parameters

The timber bridge and loading parameters are consistent for both models and are shown in Table 2.1. The number of spans is limited to two in order to keep the modeling as simple as possible while still capturing the behavior of a timber bridge. Two spans are sufficient to capture the general dynamic response. The spans are 14 feet long, which is a typical length for such bridges.

The loading is described as a freight car connection as shown in Figure 2.1. The truck on the right side of the figure supports the back half of a leading freight car, and the truck on the left supports the front half of a trailing freight car. Each axle imparts a load of 78.75 kips to the bridge, which is the maximum allowed axle load. This specific location

in the consist is chosen because it allows for the maximum amount of total load on the bridge.

The material properties are given in Table 2.2. The EI values for the stringers are simply the average values from the testing described in Section 1.7. A 136 lbs/yd rail is used to model the rail, which has standard values for E and I . The densities of the materials are given in U.S. customary units and are typical values for steel and timber. These three materials are the primary materials used for both models.

For the finite element model, geometric relationships must be defined. In the models, the ties are spaced 21 inches center to center. The rails are positioned 56.5 inches apart. The pine stringers are 8 inches wide by 16 inches deep. There are two chords of four stringers. The chords are centered underneath the rail, with the stringers in each chord placed side by side with no gaps.

2.3 Analytical Model

A two-span timber railroad bridge can be modeled as a two-span beam with point loads as shown in Figure 2.2. P represents a load traversing the beam from left to right, ξ represents the distance from the left support to the load P , and x represents the distance from the left support to any point of interest on the beam. In order to determine the deflection of the two-span beam as a function of x and ξ , the Method of Initial Parameters can be used.

Euler beam theory states that the deflection of a one-span, simply supported beam with a single point load can be represented as a function of x by:

$$w(x, \xi) = w_0 + \theta_0 x - \frac{M_0 x^2}{2EI} - \frac{V_0 x^3}{6EI} + \frac{1}{6EI} P \{x - \xi\}^3 \quad (2.1)$$

where w_0 is the initial deflection, θ_0 is the initial angle, M_0 is the initial moment, and V_0 is the initial shear. Note that $\{f(g)\}$ represents a discontinuity function, which is 0 if

negative and $f(g)$ if positive. The sign convention is such that P is positive when acting in the negative y direction.

Equation 2.1 can be applied to a two-span beam by replacing the center support by a point load, R_b . This load is fixed at a distance $L/2$ from the left support. Equation 2.1 can also be simplified by observing that M_0 and w_0 must be equal to 0 due to support conditions. Therefore, the deflection of a two span beam with a single point load can be represented by:

$$w(x, \xi) = \theta_0 x - \frac{V_0 x^3}{6EI} - \frac{R_b}{6EI} \{x - L/2\}^3 + \frac{1}{6EI} P \{x - \xi\}^3 \quad (2.2)$$

The above equation has 3 unknowns: θ_0 , V_0 , and R_b . Therefore, three independent boundary conditions are required. The three conditions are as follows:

$$w(L/2, \xi) = 0 = \theta_0 \frac{L}{2} - \frac{V_0 L^3}{48EI} + \frac{P \{L/2 - \xi\}^3}{6EI} \quad (2.3)$$

$$w(L, \xi) = 0 = \theta_0 L - \frac{V_0 L^3}{6EI} - \frac{R_b L^3}{48EI} + \frac{P(L - \xi)^3}{6EI} \quad (2.4)$$

$$w''(L, \xi) = 0 = -\frac{V_0 L}{48EI} - \frac{R_b L}{2EI} + \frac{P(L - \xi)^3}{EI} \quad (2.5)$$

These conditions represent the zero deflection at the center support, zero deflection at the right support, and zero moment at the right support. The presence of the discontinuity function in Equation 2.3 causes the three unknowns to be discontinuous. Therefore, the system of equations must be solved separately for when the load is on the left span and when the load is on the right span. If the load is on the left span, the discontinuity function is positive and must therefore be taken into account. Solving the system for the load on the left span yields the following:

$$\theta_{0,L} = \frac{P\xi}{48EIL} (7L^2 - 24L\xi + 20\xi^2) \quad (2.6)$$

$$V_{0,L} = P\left(1 - \frac{5\xi}{2L} + \frac{2\xi^3}{L^3}\right) \quad (2.7)$$

$$R_{b,L} = \frac{P\xi}{L^3}(3L^2 - 4\xi^2) \quad (2.8)$$

If the load is on the right span, the discontinuity function is negative and can therefore be set equal to zero. Solving the system for the load on the right span yields the following:

$$\theta_{0,R} = \frac{P\xi}{48EIL}(7L^2 - 24L\xi + 20\xi^2) \quad (2.9)$$

$$V_{0,R} = P\left(1 - \frac{5\xi}{2L} + \frac{2\xi^3}{L^3}\right) \quad (2.10)$$

$$R_{b,R} = \frac{P\xi}{L^3}(3L^2 - 4\xi^2) \quad (2.11)$$

The remaining issue yet to be addressed is determining an EI value to use in Equation 2.2. Instead of determining one EI value, assume that a portion of the load is carried by the rails and a portion is carried by the timber stringers. For simplicity, the stringers can be assumed to act as one beam. Therefore, the system is a bridge beam consisting of a rail beam and a stringer beam attached to one another as shown in Figure 2.2. The EI value of the rail beam is simply two times the EI value of one rail beam (there are two rails). The EI value of the stringer beam is eight times the EI value of one stringer beam (there are eight stringers).

The deflection of the rail and the deflection of the stringer can be represented by:

$$\delta_r = P_r * w_{UL,r} \quad (2.12)$$

$$\delta_s = P_s * w_{UL,s} \quad (2.13)$$

where δ_r is the deflection of the rail, δ_s is the deflection of the stringer, P_r is the load carried by the rail, P_s is the load carried by the stringer, $w_{UL,r}$ is the deflection of the rail due to a unit load, and $w_{UL,s}$ is the deflection of the stringer due to a unit load. The only difference between $w_{UL,r}$ and $w_{UL,s}$ is the EI value to be used in Equation 2.2.

In order to obtain the total bridge beam deflection, two relationships are used:

$$\delta_r = \delta_s \quad (2.14)$$

$$P_r + P_s = P \quad (2.15)$$

The first relationship simply states that the rail and the stringer deflect together. This can be assumed as long as the rail and stringer are sufficiently attached and plane sections remain plane. The second relationship states that the load carried by the rail combined with the load carried by the stringer must be equal to the total load applied. Combining Equations 2.12 through 2.15 yields the total deflection of the bridge beam:

$$\delta = \frac{(P * w_{UL,r} * w_{UL,s})}{w_{UL,r} + w_{UL,s}} \quad (2.16)$$

In order to calculate the deflection under multiple point loads, linear superposition can be applied. A δ value for each point load is calculated, and then all the δ values are added together. Therefore, as per the model parameters, four point loads can be moved over the bridge step by step. MATLAB is a useful tool for such a task, as it can rapidly calculate the deflections through the use of Boolean Logic. The code developed can be found in Appendix C.

Figure 2.4 shows how the loads move across the bridge. In the figure, P_1 and P_2 represent the first and second axle of the first rail truck, and P_3 and P_4 represent the first and second axle of the second rail truck. These two rail trucks together represent the second truck of one freight car and the first truck of a second freight-car. This type of analysis is referred to as quasi-static analysis. Note that self-weight is not considered in the analytical model.

2.4 LS-DYNA Model

LS-DYNA is a general-purpose finite element program originally developed for analyzing non-linear, dynamic problems. While the analysis for this project is linear, the explicit time integration capabilities of LS-DYNA make it ideal for conducting the dynamic analysis of the timber bridge system.

Figures 2.5 and 2.6 show an overall view and a close-up view of the LS-DYNA model. The ties are spaced 21” center to center. The rails are positioned 56.5” apart. The pine stringers are 8” wide by 16” deep. There are two chords of four stringers. The chords are centered underneath the rail, with the stringers in each chord placed side by side without gaps.

In reference to the Figures 2.5 and 2.6, red elements correspond to the rails, light blue to the timber stringers, brown to the ties, and dark blue to discrete spring elements. The black cross dots at the ends of the stringers and rails represent boundary restraints. The discrete spring elements serve to transfer the vertical load from the rails to the ties and from the ties to the stringers. These elements are specified to be very stiff, and their deformation adds no significant deflection to the bridge system. All elements besides the spring elements are Hughes-Liu beam elements with full cross-section integration. Information about Hughes-Liu elements can be found in the LS-DYNA Theory Manual (Livermore Software Technology Corporation 2007). Translational restraints acting in the X, Y, and Z directions are present on the ends of the timber stringers. Additionally, translational restraints acting in the X and Y directions are present on the ends of the rails.

The rails are extended the distance of three tie spacings past the ends of the stringers in order to more accurately model the boundary conditions of the bridge. The rail extension allows for some moment resistance to be present in the rail at the end of the bridge and for the rails to have a non-zero angle. Additionally, self-weight is added to the model.

Due to the relative lightness of a timber bridge, the self-weight does not have a large effect.

In the LS-DYNA model, the bridge is loaded by point masses as opposed to point forces. This is done by applying point masses along the rail at every intersection between rail and tie. The masses are then activated and deactivated by ramp functions. The ramp functions are constructed so that the total freight car mass is always present on the bridge. That is to say, if one quarter of the mass is on one node, then three quarters of the mass is still on the previous node. This allows the mass of the hopper to be moved across the bridge and contribute to the dynamic response of the system. Figure 2.7 shows a graphical representation of this process.

Damping is a major consideration present in the LS-DYNA model which is not present in the analytical model. Global mass proportional damping is used. LS-DYNA applies a damping force represented by:

$$F_d = D m v \quad (2.17)$$

where F_d is the damping force, m is the mass, v is the velocity, and D is the user-specified value used to control the level of damping. This is referred to as mass proportional damping because the damping matrix is replaced by the mass proportional value, Dm .

In order to determine an appropriate value for D , previous experimental testing was examined. Wipf et al. previously conducted field load testing of a timber bridge (2000). The testing found that the dynamic amplification factor (DAF) for midspan deflection of an intact timber bridge was 1.22. By definition, the DAF is the ratio of dynamic deflection to static deflection. A simple trial and error approach was used in order to determine a D value which resulted in this DAF.

2.5 Model Comparison

In order to compare all the models, a specific loading and measurement is needed. As previously discussed, the standard 4 axle load is used. The measurement of interest is the path the first axle takes as it traverses the bridge, referred to as the wheel path. To clarify, the wheel path is the vertical position of the axle on the deflected span as a function of the horizontal position of the axle on the span. The wheel path is not the deflected shape of the bridge.

In order to compare the dynamic LS-DYNA model with the static MATLAB model, the model is analyzed in LS-DYNA with a train speed of 7 inches per second (0.4 mph). This minimizes any dynamic effects and allows for a direct comparison. Additionally, the LS-DYNA model is modified to have no extended rails and no self-weight in order to achieve a closer match to the MATLAB model. Figure 2.8 shows the results from this comparison.

The results from the MATLAB model and the LS-DYNA model are within 10% of each other even though the analysis method is different. As previously mentioned, the MATLAB model serves as a benchmark for the LS-DYNA model. The fact that such agreement exists among the two models shows that the LS-DYNA model passes the benchmark test.

The next comparison made is between the LS-DYNA models with and without extended rail and self-weight. The comparison is shown in Figure 2.9. The MATLAB results are shown as well. The difference between the results from the models is at most 15%. Ultimately, the effect of different boundary conditions and self-weight are somewhat negated by each other. Extending the rail provides additional moment resistance and therefore decreases the overall bridge deflections. However, the application of self-weight causes an additional load and therefore increases the overall bridge deflections.

2.6 MATLAB and LS-DYNA Analysis Cases

In order to develop a robust SIDS, multiple train speeds with multiple damage cases need to be considered. The three train speeds being investigated are 40 mph, 30 mph, and 20 mph. For each train speed, there will be three stringer cases: fit, fully impaired, and half impaired. For the fit case, all timber stringers are considered intact and thus have intact EI values. For the fully impaired case, all timber stringers are split, and thus have split EI values. For the half impaired case, two stringers per chord are split and two are intact. The two split stringers have split EI values, and the two intact stringers have intact EI values. The EI values for intact and split stringers are shown in Table 2.2.

Results will be extracted from four observation points, referred to as Path 1, Path 2, Path 3, and Path 4. They are referred to as paths because they track the wheel paths the axles move along as the train traverses the bridge. The observations points represent each wheel and are shown in Figure 2.10.

In order to obtain accelerations from wheel paths, a three point central difference is used to find the second derivative of the path with respect to time. The equation for the central difference is given by:

$$a(x_i) = \frac{d(x_{i-1}) - 2d(x_i) + d(x_{i+1}))}{\Delta t^2} \quad (2.18)$$

where $a(x_i)$ is the acceleration at position x_i , $d(x_i)$ is the wheel path displacement at position x_i , and Δt is the time step between x_i and $x_{i\pm 1}$. A higher order method is not used because when applied to the LS-DYNA wheel path displacements, higher frequency effects start to dominate the accelerations.

CHAPTER III

MODELING RESULTS

3.1 Results from MATLAB Models

The wheel path displacements from the MATLAB models are completely independent of the train speed. Figures 3.1, 3.2, 3.3, and 3.4 show the wheel path displacements for Path 1, Path 2, Path 3, and Path 4 for any train speed. The paths are displayed as a function of position rather than time. This allows for a direct comparison between the paths. The maximum displacement for the fit stringer case is 0.271 inches. Additionally, the maximum displacement for the half impaired case is 0.342 inches, and the maximum displacement for the fully impaired cases is 0.504 inches. The greatest displacement over the first span of the bridge (0 ft. – 14 ft.) occurs in Path 2, and the greatest displacement over the second span (14 ft. – 28 ft.) occurs in Path 3.

The next graphs shown are the wheel path accelerations for all three cases. The units are in g for all cases. Note that these are the accelerations under the assumption of small angles. The train is assumed to be moving at a constant forward velocity, and therefore the time the train takes to traverse a forward distance along the bridge is considered independent of the bridge deflection. This is an important assumption when calculating the numerical derivatives.

The wheel path accelerations are only shown for a train speed of 40 mph. Figures 3.5, 3.6, 3.7, and 3.8 show the wheel path accelerations for Path 1, Path 2, Path 3, and Path 4, respectively. The only difference in accelerations for different train speeds is the specified time step in Equation 2.18. Because of this, the accelerations are inversely proportional to the square of the specified time step, and the overall shape of the acceleration curve is the exact same for any train speed.

3.2 Results from LS-DYNA Models

The first cases analyzed are the 40 mph train speed cases. Figures 3.9, 3.10, 3.11, and 3.12 show the wheel path displacements for Path 1, Path 2, Path 3, and Path 4, respectively. The maximum displacement for the fit stringer case is 0.317 inches. Comparing this to the maximum displacement obtained from the crawl case results in a DAF of 1.24. This DAF is close to the experimental value of 1.22 also discussed. The maximum displacement for the half impaired stringer case is 0.384 inches, and the maximum displacement for the fully impaired stringer case is 0.507 inches. For all three stringer cases, the greatest displacement over the first span of the bridge occurs in Path 2, and the greatest displacement over the second span occurs in Path 4.

Not shown in the figures are the markers depicting specific data points. Sixty-five data points for each path are recorded as the train traverses the bridge. At 40 mph, an observation point takes 0.48 seconds to traverse the entire bridge. Therefore sixty-five data points results in a sampling rate of about 135 data points per second.

Figures 3.13, 3.14, 3.15, and 3.16 show the wheel path accelerations for Path 1, Path 2, Path 3, and Path 4, respectively. Of note are the large negative acceleration values that occur at each end of the bridge. These values are especially amplified for the half impaired and fully impaired cases.

Figures 3.17, 3.18, 3.19, and 3.20 show the wheel path displacements for Path 1, Path 2, Path 3, and Path 4, respectively. The maximum displacement for the fit stringer case is 0.288 inches. Comparing this with the crawl case results in a DAF of 1.13. As expected, this is smaller than the DAF for the 40 mph train speed. The maximum displacement is 0.502 inches for the fully impaired case and 0.371 inches for the half impaired cases. As for the 40 mph cases, the greatest displacement for all stringer cases occurs in Path 2 for the first span and Path 4 for the second span.

The next graphs shown are the wheel path accelerations for all three cases. Figures 3.21, 3.22, 3.23, and 3.24 show the wheel path accelerations for Path 1, Path 2, Path 3, and Path 4, respectively. The scale for the graphs is half the scale of the 40 mph acceleration graphs. Since the train is moving at a slower speed across the bridge, the accelerations are lower. The overall shapes of the acceleration graphs are similar to the 40 mph cases.

The next cases analyzed are the 20 mph train speed cases. Figure 3.25, 3.26, 3.27, and 3.28 show the wheel path displacements for Path 1, Path 2, Path 3, and Path 4, respectively. The maximum displacement for the fit stringer case is 0.272 inches. Comparing this with the crawl case results in a DAF of 1.07. As expected, this is smaller than the DAFs for the 40 mph and 30 mph train speeds. The maximum displacement is 0.470 inches for the fully impaired case and 0.345 inches for the half impaired cases. As for the 40 mph and 30 mph cases, the greatest displacement for all stringer cases occurs in Path 2 for the first span and Path 4 for the second span. Additionally, Figures 3.29, 3.30, 3.31, and 3.32 show the wheel path accelerations for Path 1, Path 2, Path 3, and Path 4, respectively.

CHAPTER IV

NEURAL NETWORK DEVELOPMENT

4.1 Overview of Neural Network Development

Three sets of neural networks are developed. The first set of networks is developed with acceleration input from only the MATLAB results, the second set with acceleration input from only the LS-DYNA results, and the third set with acceleration input from both the MATLAB and LS-DYNA results. A set of networks is defined as containing a separate neural network for all combinations of the four wheel paths and three train speeds. Therefore, a set contains 12 total networks. The motivation for developing separate sets of networks is to investigate how effective different model data are in determining the structural fitness of the bridge.

The neural network toolbox available in MATLAB is used to develop the networks. The toolbox offers a wide variety of settings and options for setting up neural networks. Additionally, the training algorithms used for the networks have been optimized to provide faster training.

4.2 Network Architecture

The general network architecture used is the same for all the networks developed and is shown in Figure 4.1. The input vectors are sixty-five rows by one column acceleration vectors obtained from the modeling results. The acceleration vector is passed through two hidden layers of neurons and then output as a two rows by one column bridge condition vector. The rationale for choosing this architecture is to progressively go from the acceleration vector with sixty-five quantities to the output vector with only two quantities. This is also the rationale for having sixteen neurons in the first hidden layer and four neurons in the second hidden layer.

There are three possible bridge condition vectors as shown in Figure 4.2. The first option is “fit,” represented by [1; 0]. The second option is “half impaired,” represented by [1; 1]. The third and final option is “fully impaired,” represented by [0; 1].

The transfer functions contained in the hidden layers are logsig functions for all the neurons in all the networks. The logsig function is used because the output of the logsig function is a value between zero and one, which matches the range of the output vector. The function is shown in Figure 4.3.

As a general rule, neural networks tend to train better with as few neurons and hidden layers as possible. Furthermore, neural networks need a large enough number of neurons and hidden layers in order to establish the relationship among the input vector and the output vector.

4.3 Creating Training and Testing Vectors

In order to properly train and test the neural networks, multiple training and testing vectors are created by adding noise to the pure acceleration vectors obtained from modeling. The noise is meant to simulate unaccounted for dynamic effects as well as some random variation in the dynamic characteristics of the system. White Gaussian noise is used, which is simply noise that follows a normal distribution. The specified standard deviation is 0.075g. This means that 68.27% of the noise should fall within plus or minus 0.075g. An example of an acceleration vector with noise added is given in Figure 4.4.

The value of 0.075g is roughly 20% of the maximum acceleration obtained from the LS-DYNA results with a 40 mph train speed and a fit bridge. With this amount of noise added, the signal is distorted enough to provide a reasonable challenge for the network but still be intact enough to be recognizable. Worth noting is that the range of noise added is the same for all the train speed cases. Recall from the modeling results that the

slower the train, the smaller the accelerations. As a result of this relationship, the signal to noise ratio is smaller for slower train speeds, meaning that the signal is more distorted. This is appropriate because much of the noise picked up from actual sensors is likely to be independent of train speed. In order to simulate actual conditions, noise independent of train speed is added.

4.4 Training and Testing the Networks

Thirty training vectors are created for each network. Ten vectors are created from the fit accelerations, ten from the half impaired accelerations, and ten from the fully impaired accelerations. As stated before, a separate network is created for each wheel path and train speed combination obtained from each set of modeling results. The network is given the set of thirty training vectors with the matching bridge condition vectors. Then, the network iteratively adjusts the weights until the network produces the matching bridge conditions to a specified tolerance.

In order to test the networks, thirty separate testing vectors are created. These vectors are created from adding white Gaussian noise to the same pure acceleration vectors from which the training vectors are produced. While similar to the training vectors, the test vectors are different enough to test if the neural networks are able to create an adequate correlation between the input vectors and the output vectors. The test vectors are inputted into the network, and then the output vector is compared to what the output should be.

4.5 Agreement Criterion for Determining Bridge Condition

In order to better utilize the fact that four separate paths are being analyzed, an agreement criterion for determining the actual bridge condition can be established. A determination of bridge condition is only made when three out of the four outputs from the four separate wheel path networks are the same. For example, the networks for Path 1 and Path 2 may output the vector corresponding to a fit bridge while the networks for

Path 3 and Path 4 may output the vector corresponding to a half impaired bridge. Since there is no majority agreement on the output vector, an overall determination of bridge condition cannot be made. As another example, the networks for Path 1, Path 2, and Path 3 may output the vector corresponding to a fully impaired bridge while the network for Path 4 outputs the vector corresponding to a fit bridge. The determination of bridge condition for this example would be that the bridge is fully impaired.

CHAPTER V

NEURAL NETWORK RESULTS

5.1 Explanation of Table Structure

The data are displayed to show the percentage of correct outputs for certain types of bridge conditions. For example, examine the row labeled “Path 1” in Table 5.1. One network was trained for Path 1 data which covered all three bridge conditions: fit, half impaired, and fully impaired. The network was then tested with data covering all three bridge conditions. When tested, the network was able to select the correct output vector 93% of the time when given a fit bridge acceleration vector, 60% of the time when given a half impaired bridge acceleration vector, and 100% of the time when given a fully impaired bridge acceleration vector.

The last two rows of each table are labeled as “A.C. Correct” and “A.C. Incorrect.” A.C. stands for Agreement Criterion, and the two rows show the percentage of correct and incorrect bridge condition determinations using the majority vote process discussed in section 4.5.

5.2 Networks from 20 mph Train Speed Cases

Many neural networks failed to adequately train when given data from a train moving at 20 mph. More specifically, the networks failed to train within the specified tolerance within an appropriate number of training iterations. The tolerance and iteration limits could be relaxed, but this would compromise the accuracy of the neural networks. Additionally, on the occasions when the networks did train to within the specified tolerance, the testing results were abysmal. Specifically, the testing results failed to produce any significant number of correct vector outputs, and often times the vector outputs were completely out of the range of zero to one. Section 6.3 discusses the failure of these networks in greater detail.

5.3 MATLAB Acceleration Input Networks

Tables 5.1 and 5.2 show the percentage of correct outputs for the networks trained on MATLAB acceleration input for 40 mph and 30 mph train speeds, respectively. When using the agreement criterion previously discussed, the 40 mph networks were able to determine the correct bridge condition 90% of the time and were incorrect only 2% of the time. The 30 mph networks were able to determine the correct bridge condition 79% of the time and were incorrect 4% of the time.

5.4 LS-DYNA Acceleration Input Networks

Tables 5.3 and 5.4 show the percentage of correct outputs for the networks trained on LS-DYNA acceleration input for 40 mph and 30 mph train speeds, respectively. When using the agreement criterion, the 40 mph networks were able to determine the correct bridge condition 99% of the time and were incorrect 0% of the time. The 30 mph networks were able to determine the correct bridge condition 91% of the time and were incorrect only 1% of the time.

5.5 Combined MATLAB and LS-DYNA Acceleration Input Networks

Tables 5.5 and 5.6 show the percentage of correct outputs for the networks trained on combined MATLAB and LS-DYNA acceleration input for 40 mph and 30 mph train speeds, respectively. When using the agreement criterion, the 40 mph networks were able to determine the correct bridge condition 90% of the time and were incorrect only 1% of the time. The 30 mph networks were able to determine the correct bridge condition 70% of the time and were incorrect only 7% of the time.

Overall, the networks were able to determine the correct bridge condition 87% of the time and were incorrect 3% of the time. The networks trained with only LS-DYNA acceleration input with a 40 mph train speed exhibited superior performance. The networks trained with combined acceleration input with a 30 mph train speed were less successful.

CHAPTER VI

DISCUSSION

6.1 Displacements and Accelerations from MATLAB Model

The displacements obtained from the MATLAB model are shown in Figure 3.1, 3.2, 3.3, and 3.4. The displacements of Path 1 and Path 4, as well as Path 2 and Path 3, mirror each other across the middle support of the bridge. This is a result of no dynamic effects and the symmetric spacing of the axles. Path 2 has the greatest displacement over the first span, though only slightly. Additionally, Path 3 has the greatest displacement over the second span.

It is important to note that the displacements are independent of train speed due to the quasi-static analysis method. The train speed is specified by the time step used for the numerical differentiation in Equation 2.18. The faster the train speed, the shorter the time step, and therefore the greater the acceleration. Since the time step is squared due to taking the second derivative, the accelerations are proportional to the square of the train speed.

Note the kinks that are present in all the path displacements. As an example, refer to Figure 3.1 at a position of about 6 feet where the curve suddenly changes direction. This behavior shape in the curve is referred to as a “kink.” Every time an axle load comes on or leaves the bridge, a kink occurs in all paths present on the bridge. These kinks have a major effect on the accelerations because the derivative at a kink is undefined. When the numerical differentiation is carried out, the values at these kinks are extremely high. As the time step approaches zero, the acceleration value approaches infinity. Therefore, the accelerations at these points are manually deleted before being fed into the neural networks in order to achieve better network performance. Even though the networks are somewhat able to handle the acceleration spikes, the overall performance is lower when the spikes are not deleted.

As expected, the displacements and accelerations are both significantly different depending on the structural fitness of the bridge. The relative difference between the displacements stays consistent throughout the path, and as a result the absolute difference is greatest whenever the displacement is greatest. The same occurs with accelerations. Overall, five relative minima and maxima exist for both displacements and accelerations. The extrema are located at the beginning of the bridge, the midspan of the first span, the center support, the midspan of the second span, and the end of the bridge.

6.2 Displacements and Accelerations from the LS-DYNA Models

The results obtained from the LS-DYNA models are more varied than the MATLAB results due to dynamic effects as well as varying train speeds. The greater the train speed, the greater the DAF. However, the dynamic amplification factor is relatively small, even when the train speed is 40 mph. This is due to the large amount of damping present in the system. The magnitude of the accelerations is more dependent on the train speed itself than the actual DAF. The reason for the dependence on the train speed is the same as before: the faster the train speed, the shorter the time step and therefore the greater the acceleration.

The dynamic effects are best exemplified when comparing the LS-DYNA results to the MATLAB results. For the comparison, consider the second wheel path of a fit bridge with a train speed of 40 mph. Figure 6.1 shows the wheel path displacements from the LS-DYNA results in red and the MATLAB results in blue. The main difference is the minor phase shift between the displacement curves. This shift is due to the dynamic characteristics of the system: mass, stiffness, and damping. Additionally, the DAF causes the displacement to be greater for the LS-DYNA curve.

Figure 6.2 shows the wheel path accelerations from the LS-DYNA results and the MATLAB results. There is a bigger disparity in the acceleration curves than in the displacement curves. The LS-DYNA acceleration curve oscillates while the MATLAB

curve is smooth. Additionally, the same phase shift from the displacement curves is present. Even though these obvious differences exist, the curves are quite similar. This similarity indicates that neural networks can be trained using results from both models.

6.3 The Effect of Train Speed on Acceleration and Network Performance

Figure 6.3 shows a direct comparison of acceleration signals obtained from an LS-DYNA, fit bridge. Note that when plotted with 30 mph and 40 mph acceleration signals, the 20 mph signal appears almost as a flat-line. As previously stated, the acceleration is proportional to the square of the train speed. Therefore, the range of the 20 mph acceleration signal is approximately one fourth the range of the 40 mph acceleration signal.

The 20 mph train speed networks are not successful. The main cause of failure for the 20 mph networks is the lower signal to noise ratio when compared to the 30 mph and 40 mph networks. The same level of noise is given to all the networks, despite train speed. If less noise is given to the 20 mph accelerations, then the networks are able to train and produce adequate outputs. However, acceleration noise must be taken into account when training and simulating the neural networks. Noise represents unaccounted for dynamic effects and random variation of the dynamic characteristics of the system. Much of this noise is expected to be independent of train speed. It is the opinion of the author that any reasonable amount of noise would dominate the signal obtained from a train moving at 20 mph. Actual experimentation would confirm or refute this opinion.

6.4 The Effect of Load Magnitude on Accelerations

Figure 6.4 shows a comparison between accelerations obtained from the MATLAB model of a fit bridge and a train speed of 40 mph. The acceleration curve labeled as “half load” is obtained from an analysis using only half the full freight car load. The acceleration range of the half load case is one half the range of the full load case. Clearly, acceleration is directly proportional to the magnitude of the load. Therefore,

heavier freight cars result in larger acceleration ranges and higher signal to noise ratios. However, the effect of the load is not as great as the effect of the train speed.

6.5 General Neural Network Performance

The 40 mph and 30 mph train speed networks are generally successful in producing the correct outputs when given acceleration vectors with added noise as inputs. In part, success is dependent on the path from which the training vectors are obtained. The networks trained on Path 1 and Path 4 vectors are less successful than the networks trained on Path 2 and Path 3 vectors. However, the difference in success is offset by requiring three out of four paths to agree when determining the bridge condition. Overall, all four paths are useful in the development of the SIDS.

The 40 mph networks perform better than the 30 mph networks. In fact, the 40 mph networks are correct at least 90% of the time and incorrect at most 2% of the time. Recall that the faster the train speed, the greater the acceleration values and thus the greater the signal to noise ratio. The higher signal to noise ratio leads to the 40 mph performing better than the 30 mph networks. The main failing of the 30 mph networks is in the percentage of correct determinations after applying the agreement criterion. However, the 30 mph networks rarely determine the wrong bridge condition; they simply fail to come to an agreement on any bridge condition at all. Even though the percentage of correct outputs is as low as 70% in Table 5.6, the networks are only incorrect 7% of the time. This low percentage of incorrect determinations makes both the 40 mph and 30 mph networks useful in the development of the SIDS.

The success of the networks is also dependent on the type of bridge condition from which the acceleration vectors are obtained. When given acceleration vectors from half impaired bridges, the neural networks perform significantly worse than when given acceleration vectors from fit or fully impaired bridges. The networks tend to perform much better when given an acceleration vector from one extreme or the other. When a

network produces an incorrect output, that incorrect output is almost always one choice away from the correct output. For example, the networks almost never output that the bridge is fit when it is in fact fully impaired, and vice versa.

When comparing the performance of the networks according to different types of model input, the order of success from superior to inferior performance: 1) LS-DYNA input only, 2) MATLAB input only, and 3) combined input. The reason for the superior performance of the LS-DYNA input networks over the MATLAB input networks is not entirely clear. One possible reason could be that the LS-DYNA acceleration curves appear to oscillate more when impairment is added. The combined input performs only slightly worse than the MATLAB input.

The fact that the networks can train on input from two separate models, one quasi-static and one dynamic, is quite remarkable. This capability to produce correct outputs when given combined input is more important than the capability to produce correct outputs when given an acceleration vector with noise from only one type of input. The precise dynamic characteristics of any given timber bridge would be nearly impossible to find. However, these precise characteristics are not necessary in the development of the SIDS. In fact, the quasi-static model that only considers the stiffness of the system is very compatible with the LS-DYNA model that considers mass, damping, dynamic amplification, and vibration effects. This compatibility indicates that an experimental SIDS could indeed be developed for any set of timber bridges with the same general geometric properties.

CHAPTER VII

CONCLUSIONS

7.1 Conclusions

The ability of the neural networks to correctly determine bridge condition when trained and tested on results from two different models, one quasi-static and one dynamic, shows that the Structural Impairment Detection System developed in this paper is viable. Furthermore, the methodology developed could be applied to the development of an experimental SIDS. An overview of the methodology is as follows:

- 1) Obtain wheel path accelerations from freight cars traversing timber railway bridges with various levels of known bridge conditions.
- 2) Set aside some wheel path accelerations for training and some for testing.
- 3) Train neural networks to link the training set of accelerations to the known bridge conditions.
- 4) Simulate the neural networks on the simulation set of accelerations.
- 5) If the testing of the network is successful, then the SIDS has been properly developed and can be used to determine the condition of any similar timber railway bridge with traffic.

7.2 Future Research

More theoretical research could be conducted in order to investigate the effects of more spans, pile deformations, different types of loading, different train speed, more or less stringers, different geometry, etc. However, the value of further theoretical research pales in comparison to the value of actual experimental testing. The procedures discussed in this paper demonstrate the general methodology of how to develop a SIDS, and the results show that it is theoretically possible. Future research should focus on conducting experimental research on one or more test bridges. Bridges with different levels of impairment should be investigated. The practical aspects of placing

accelerometers on loaded freight cars should also be explored. In addition, the test bridges should be instrumented with string potentiometers or some other type of device in order to measure the deflections due to freight car loads.

REFERENCES

- Emerson, R.N., Pollock, D.G., Kainz, J. A., Fridley, K.J., McLean, D.I., and Ross, R.J. (1998). "Nondestructive Evaluation Techniques for Timber Bridges." *Proc., 5th World Conference on Timber Engineering*, Monteaux, Switzerland.
- Federal Highway Administration (2009). "National Bridge Inventory." <<http://www.fhwa.dot.gov/bridge/nbi.htm> > (19 August 2010).
- Fry, G.T., Comardo, A.F., Uppal, A.S., and Otter, D. E. (2000). "Fatigue Strength of Treated Southern Pine Timber Railroad Bridge Stringers." *Research Publication TD-00-019*, Association of American Railroads/Transportation Technology Center, Inc., Pueblo, CO.
- Hagan, H.T., Demuth, H.B., and Beale, M. (1996). *Neural Network Design*. PWS Publishing Company, Boston, MA.
- Lee, J.W., Kirikera, G.R., Kang, I., Schulz, M.J., and Shanov, V.N. (2006). "Structural Health Monitoring Using Continuous Sensors and Neural Network Analysis." *Smart Materials and Structures*, 15(5), 1266-1274.
- Li, H., Sun, H., and Song, G. (2004). "Damage Diagnosis of Framework Structure Based on Wavelet Packer Analysis and Neural Network." *Proc., SPIE 5391*, San Diego, CA, USA.
- Moreu, F. and Nagayama, T. (2008). "Use of Wireless Sensors For Timber Trestle Railroad Bridges Health Monitoring Assessment." *Proc., 2008 Structures Congress*, Vancouver, Canada.

- Morison, A., VanKarsen, C.D., Evensen, H.A., Ligon, J.B., Erickson, J.R., Ross, J.R., and Forsman, J.W. (2002). "Timber Bridge Evaluation: A Global Nondestructive Approach Using Impact Generated FRFs." *Proc., 20th International Modal Analysis Conference*, Los Angeles, CA, USA.
- Peterson, M.L., and Gutkowski, R.M. (1997). "Evaluation of the Structural Integrity of Timber Bridges." *NDT&E International*, 32(1), 43-48.
- Radford, D.W., Van Goethem, D., Gutkowski, R.M., and Peterson, M.L. (2002). "Composite Repair of Timber Structures." *Construction and Building Materials*, 16(7), 417-425.
- Rosenblatt, F. (1958). "The Perceptron: A probabilistic model for information storage and organization of the brain." *Psychological Review*, 65(g), 386-408.
- Wipf, T.J., Ritter, M.A., and Wood, D.L. (2000). "Evaluation and Field Load Testing of Timber Railroad Bridge." *Proc. 5th International Bridge Engineering Conference*, Tampa, FL, USA.

APPENDIX A
FIGURES

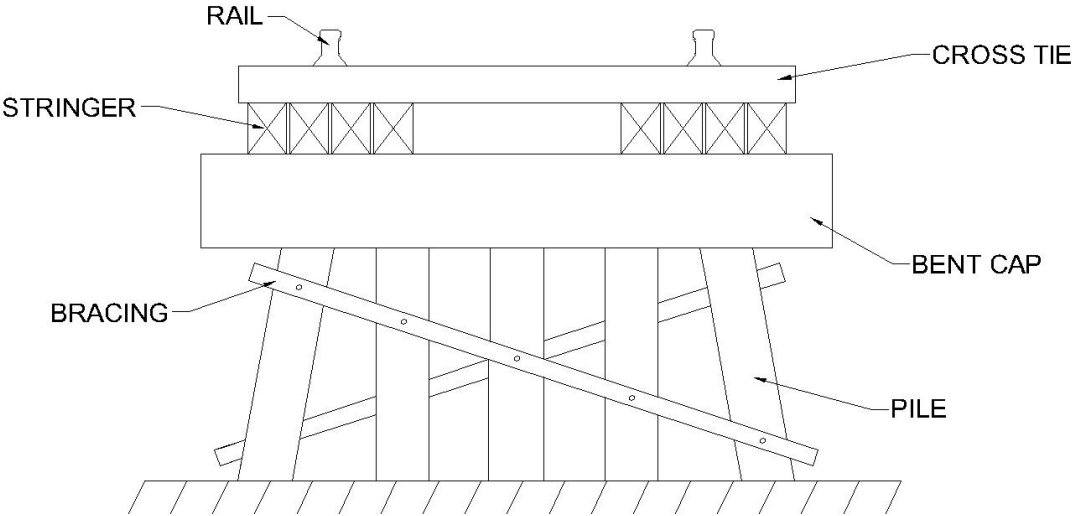


Fig. 1.1 Typical cross section of a timber railroad bridge

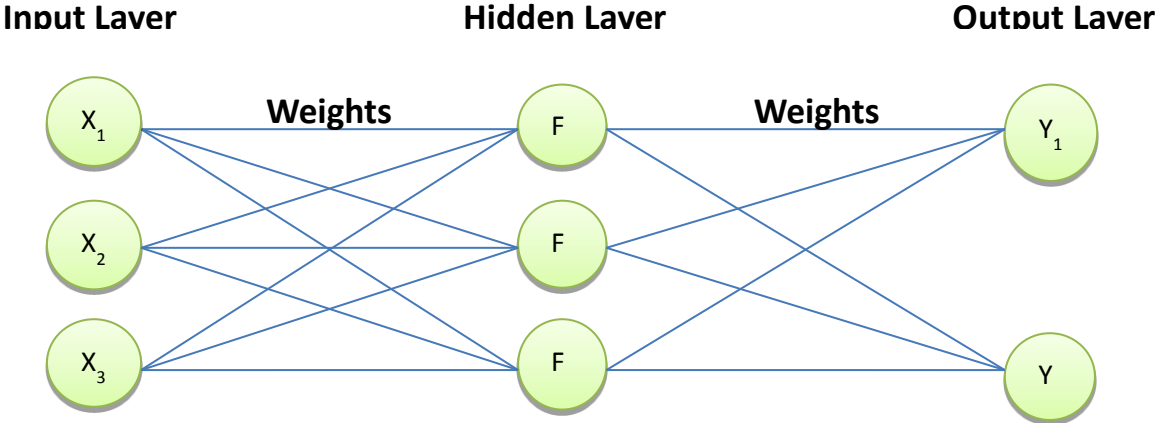


Fig. 1.2. Example of a multi-layer perceptron



Fig 1.3. Timber stringer with typical horizontal shear crack

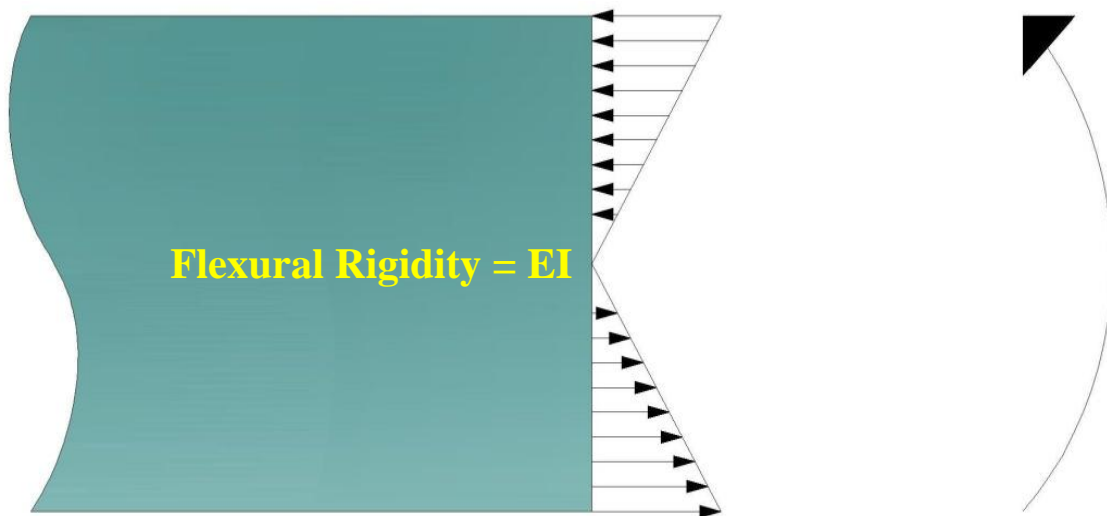


Fig. 1.4. Stress distribution of intact beam

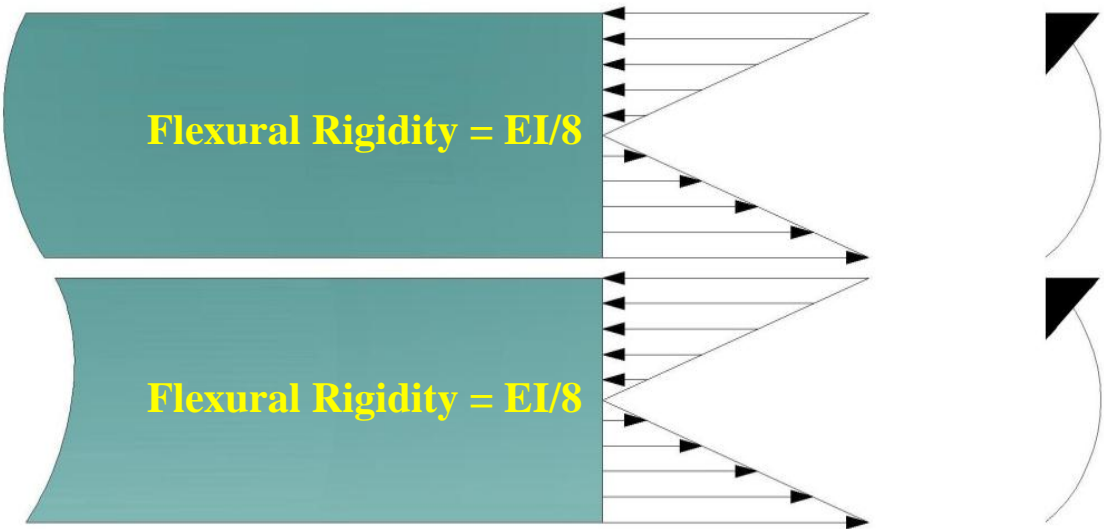


Fig 1.5. Stress distribution in a cracked beam

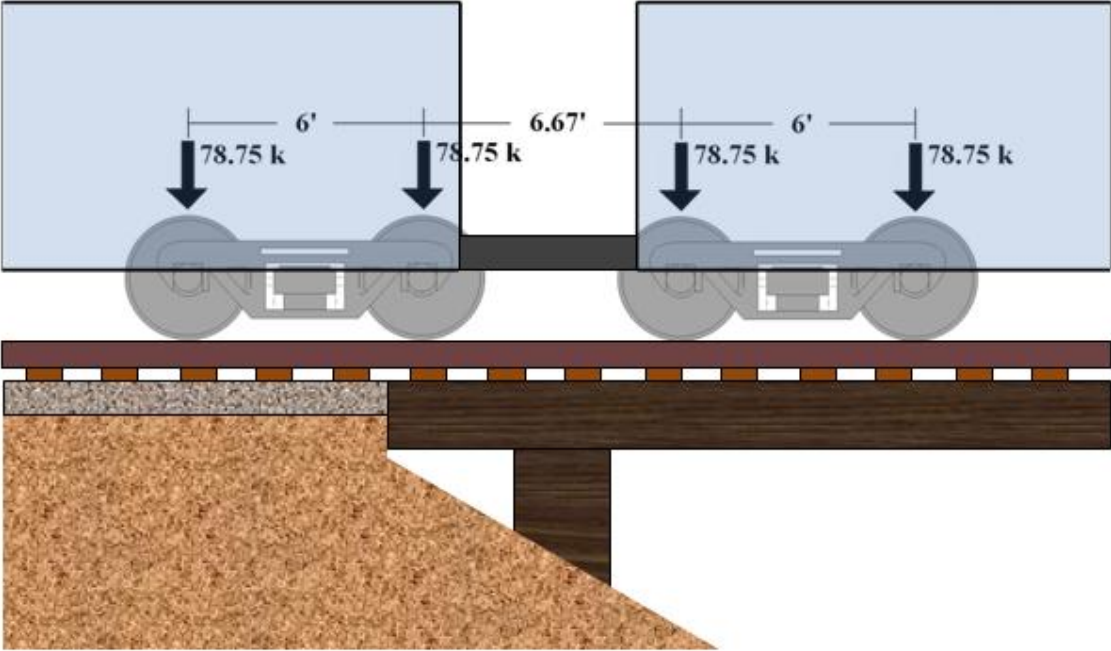


Fig 2.1. Freight car connection load

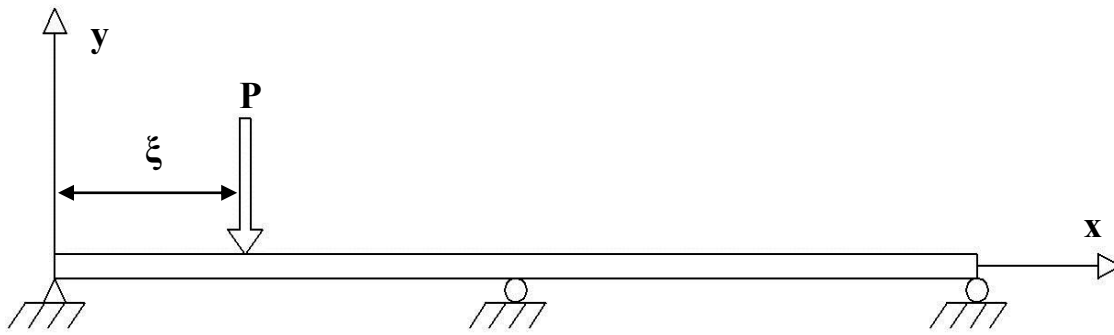


Fig. 2.2. Two-span beam representing a timber railway bridge

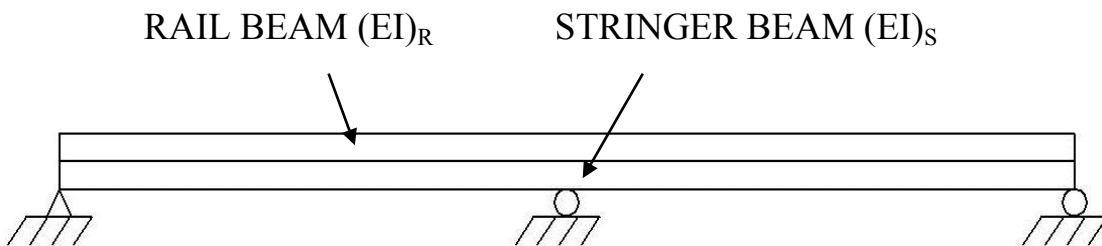


Fig 2.3 Bridge model consisting of a rail beam and a stringer beam

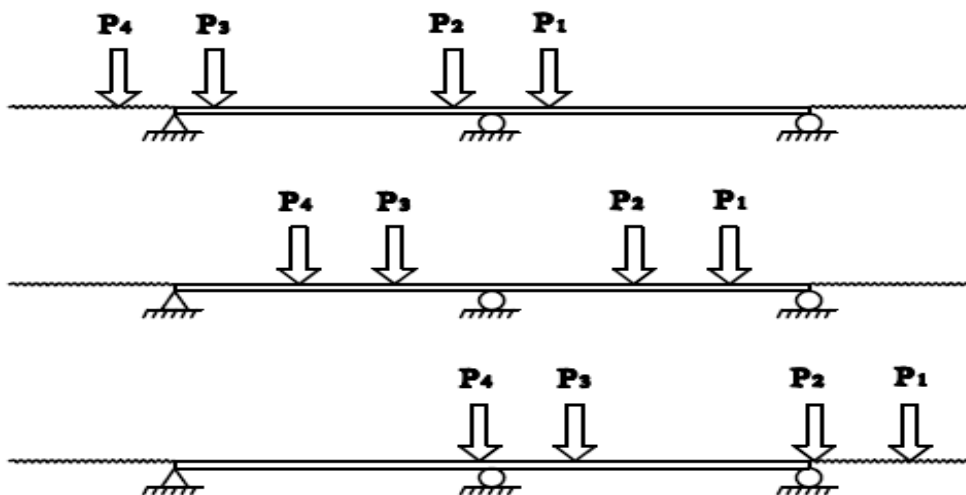


Fig 2.4. Four axle loads traversing two-span bridge

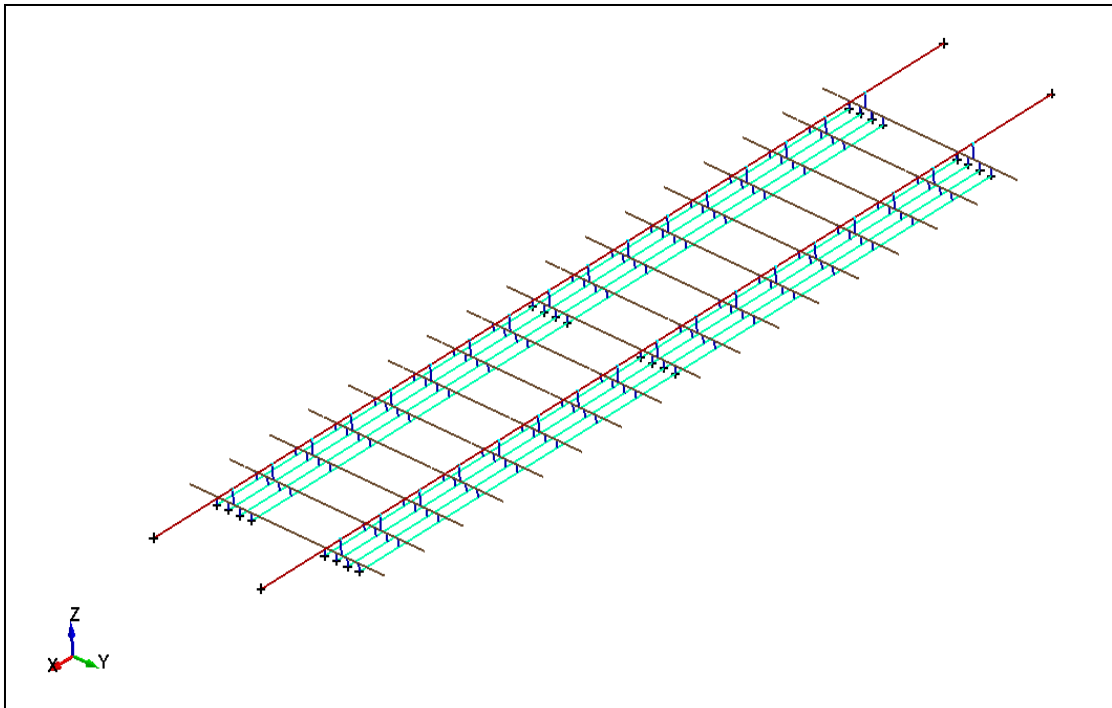


Fig 2.5. Overall view of the LS-DYNA model

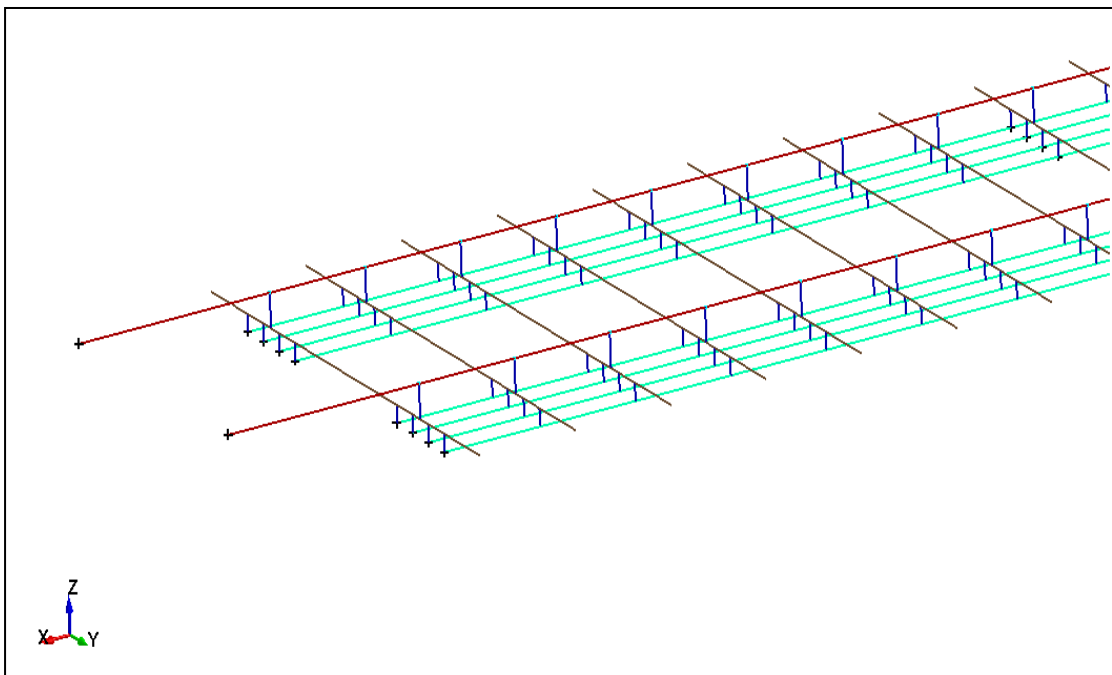


Fig 2.6. Close-up view of one half of the LS-DYNA model

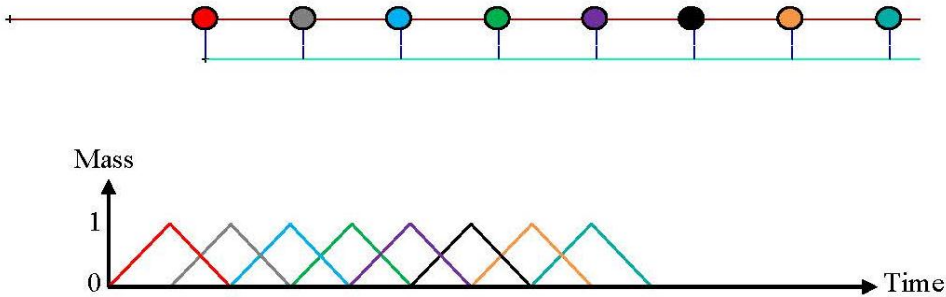


Fig 2.7. Point masses controlled by ramp functions

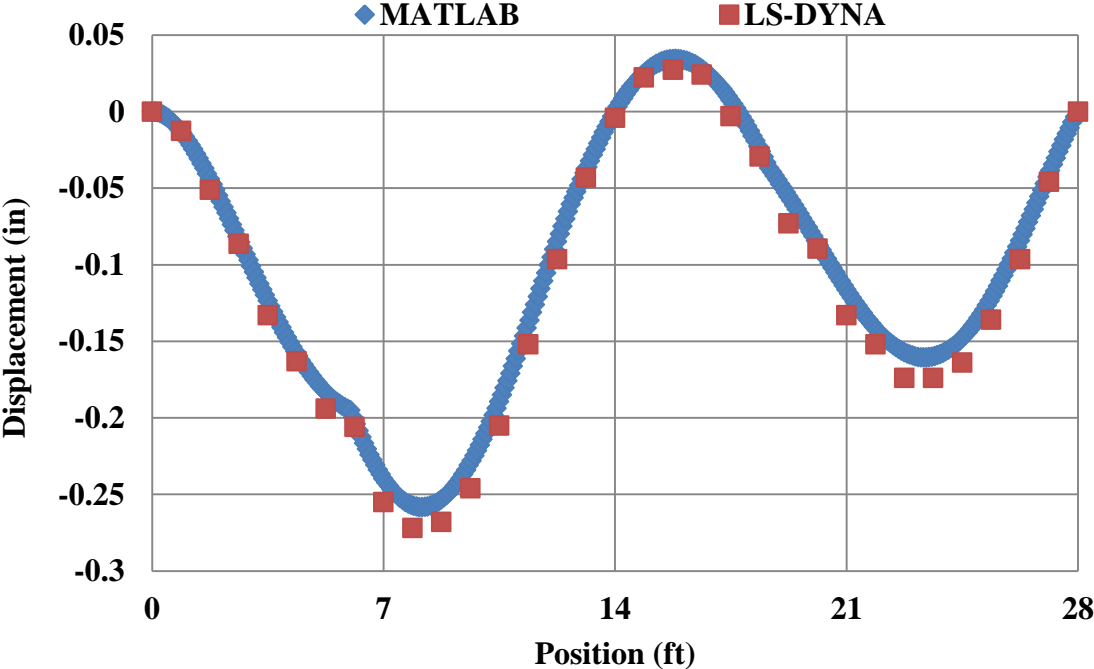


Fig. 2.8. Comparison of models – 1st wheel path

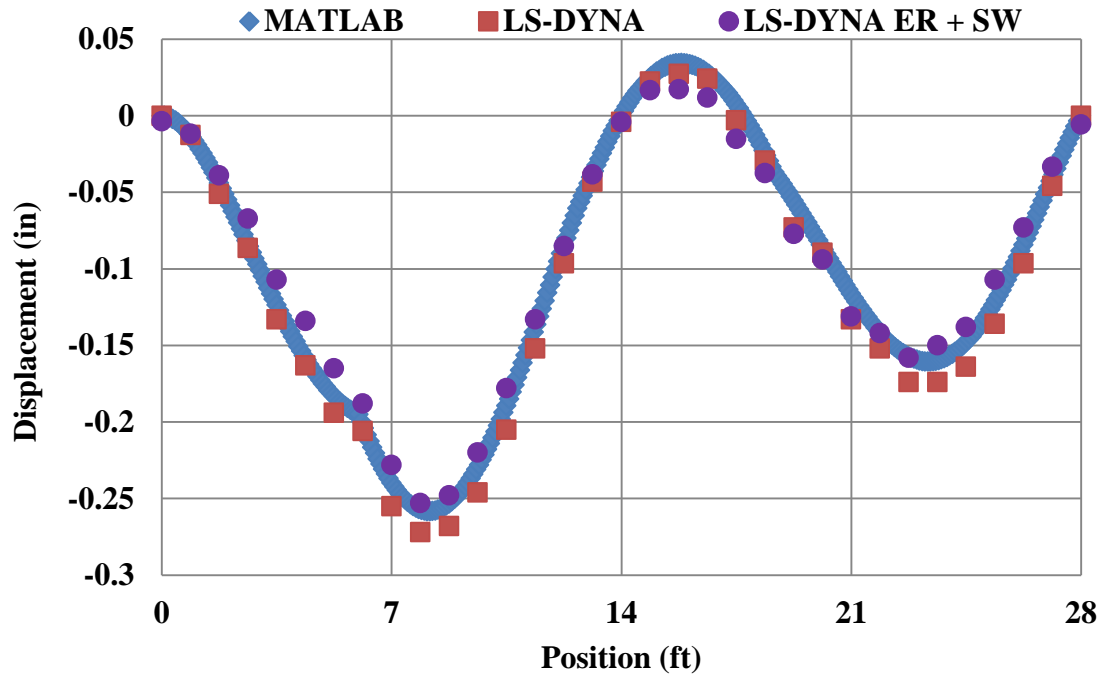


Fig 2.9. Effect of extended rails (ER) and self-weight (SW)

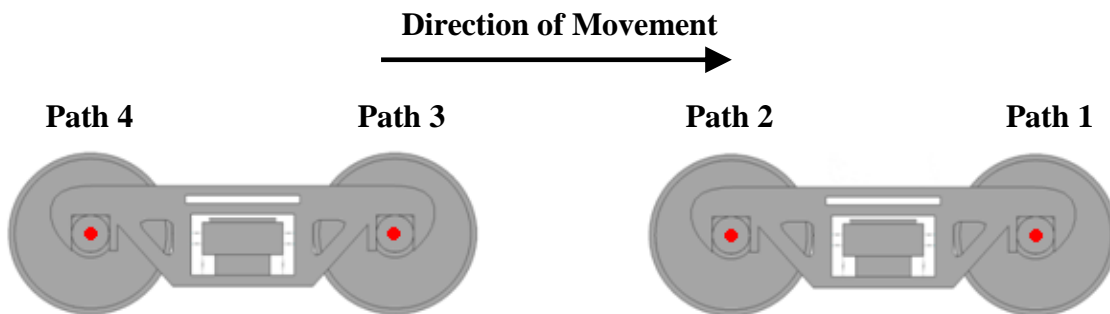


Fig 2.10. Observation points

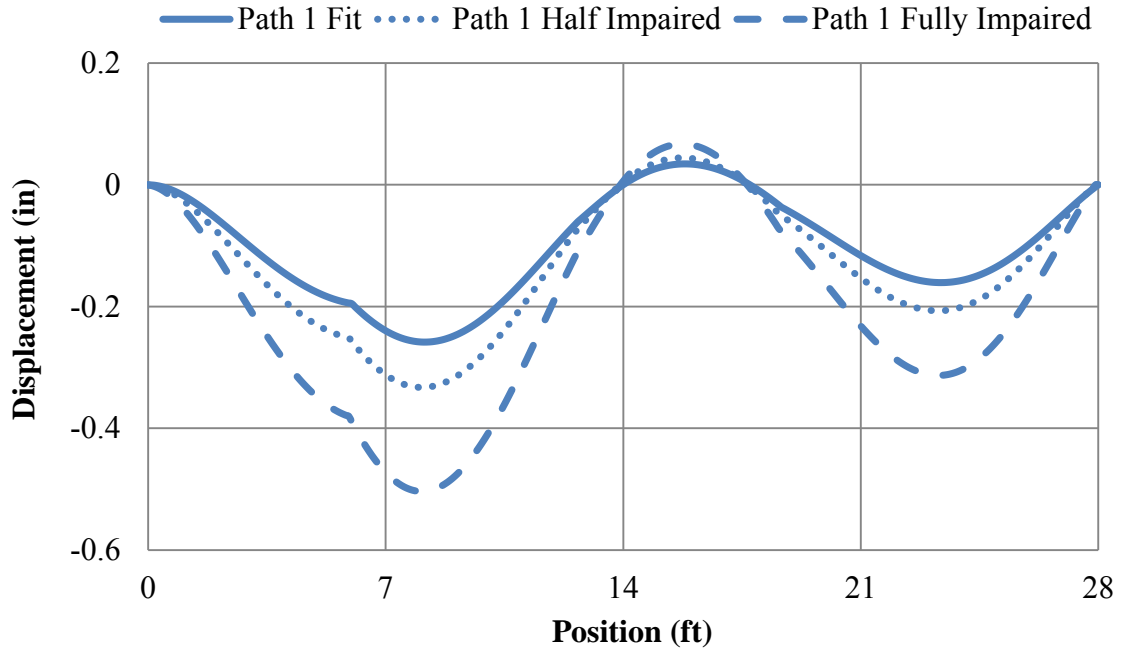


Fig. 3.1. Path 1 MATLAB wheel path displacements

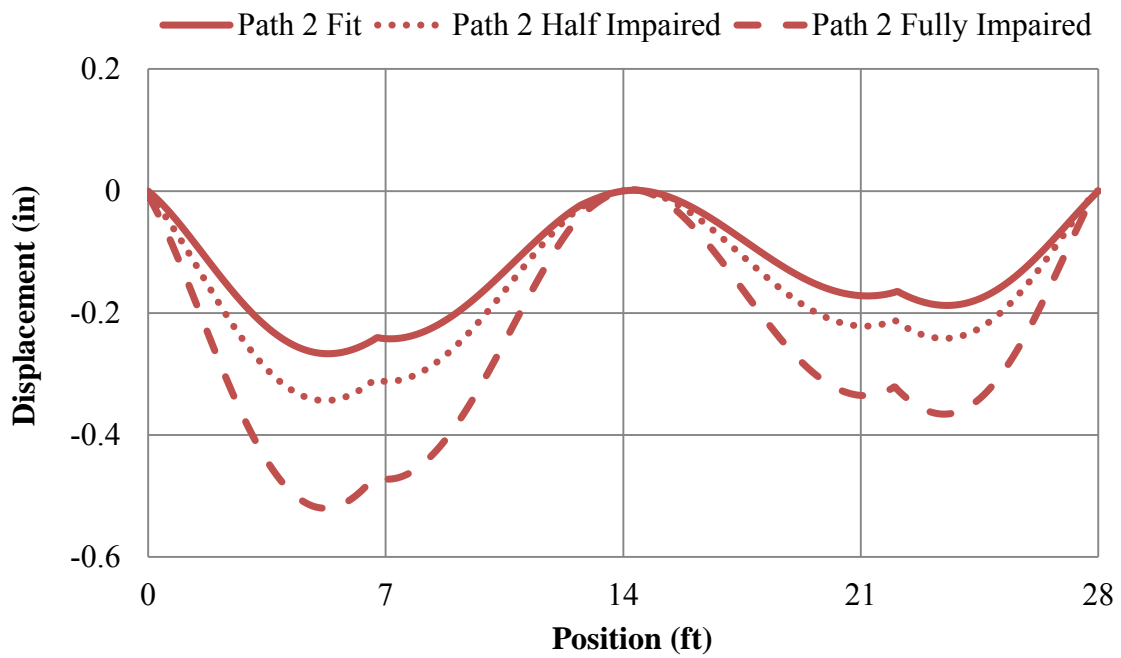


Fig. 3.2. Path 2 MATLAB wheel path displacements

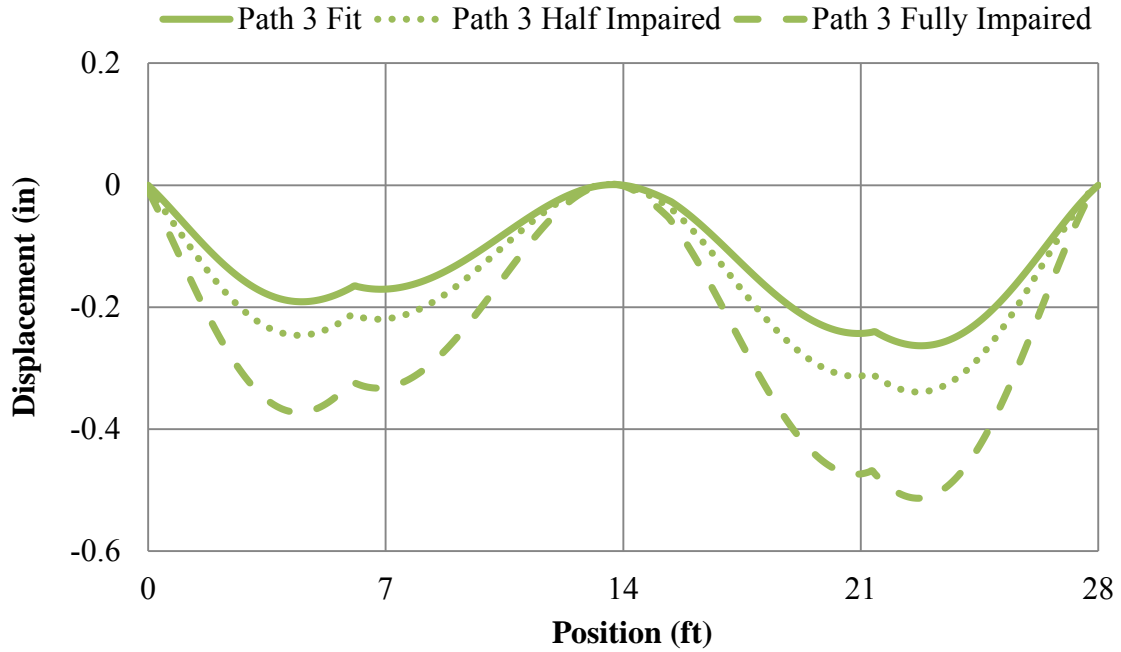


Fig. 3.3. Path 3 MATLAB wheel path displacements

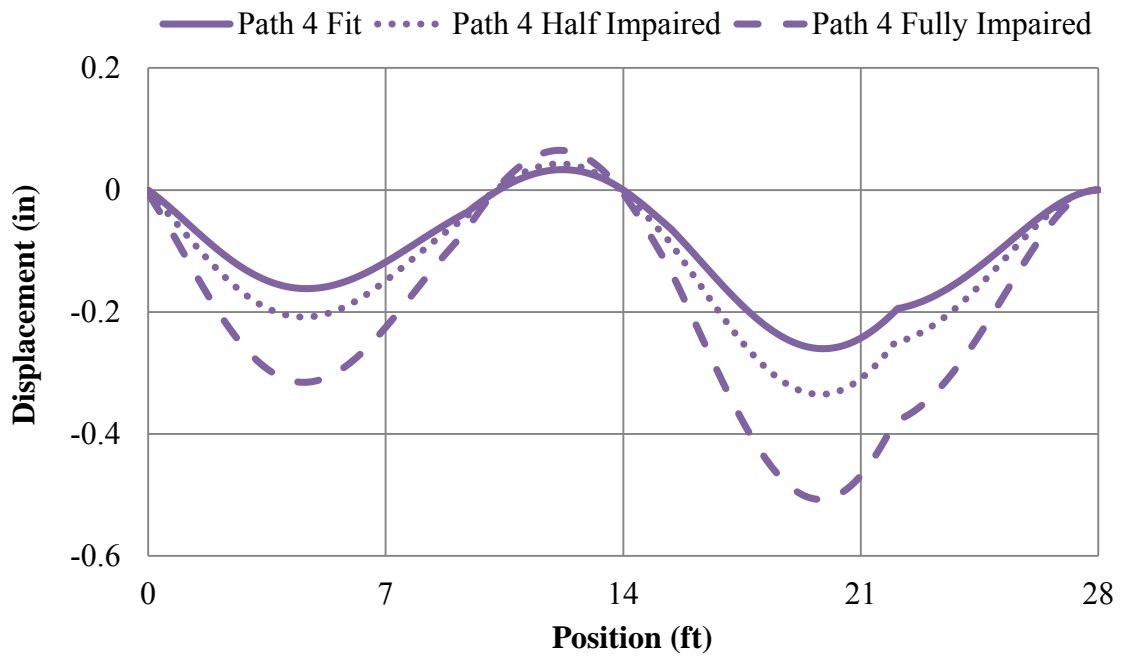


Fig. 3.4. Path 4 MATLAB wheel path displacements

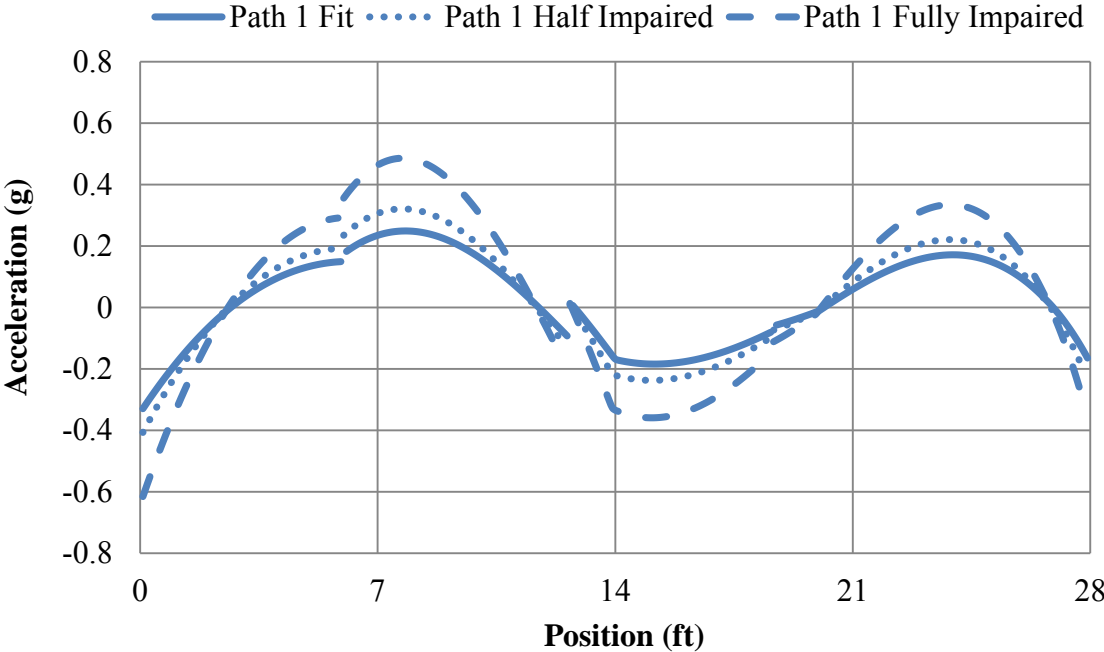


Fig. 3.5. Path 1 MATLAB wheel path accelerations – 40 mph

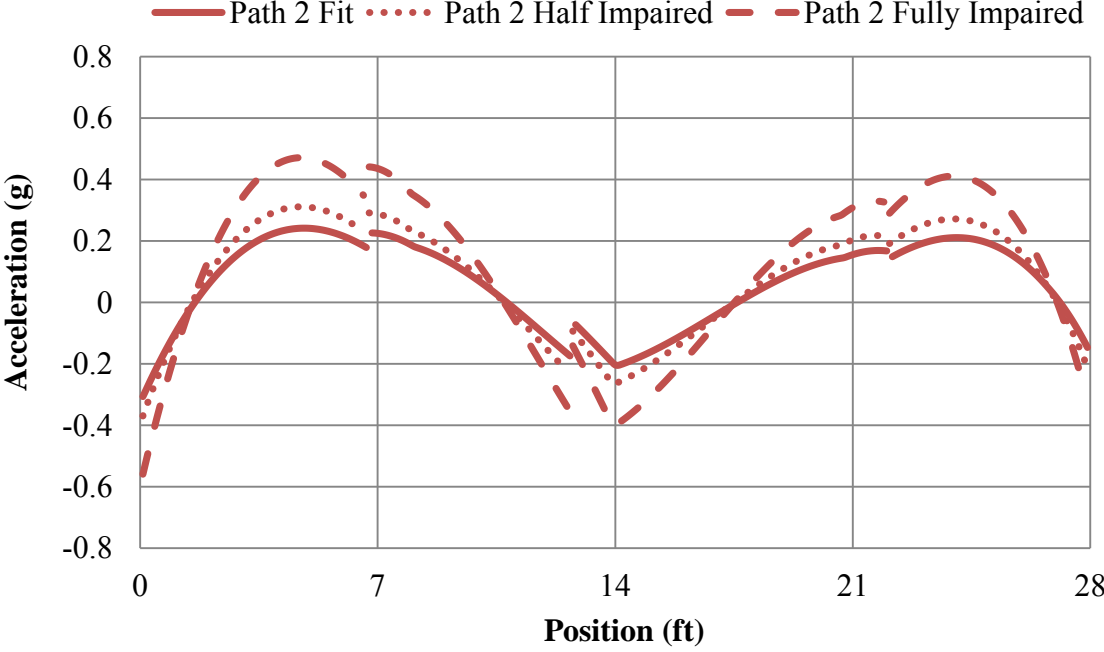


Fig. 3.6. Path 2 MATLAB wheel path accelerations – 40 mph

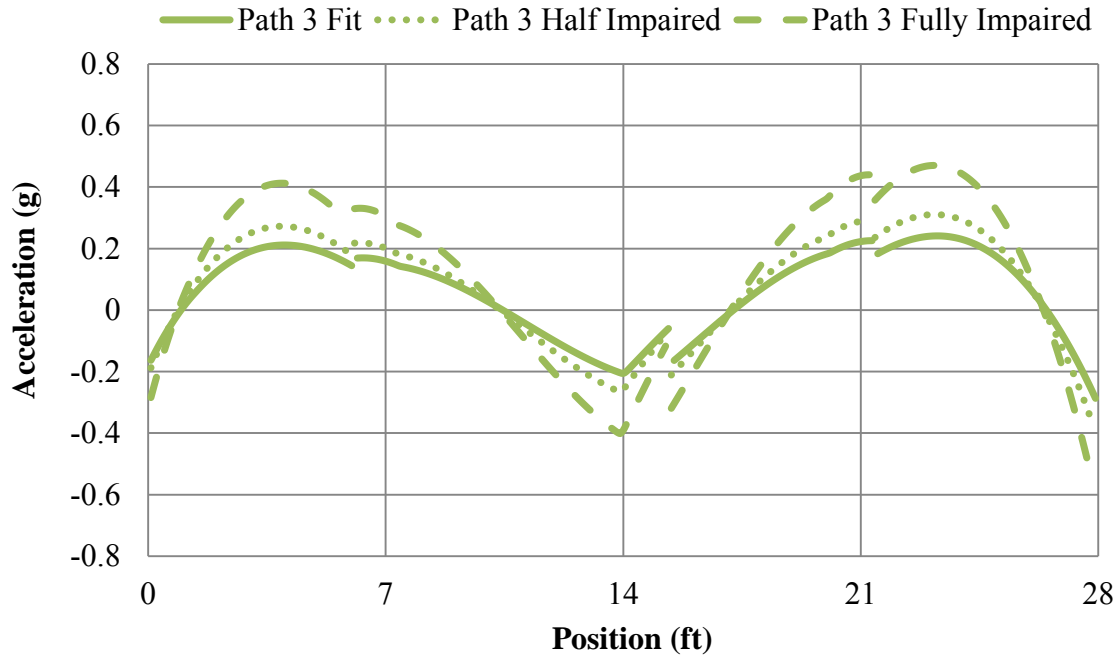


Fig. 3.7. Path 3 MATLAB wheel path accelerations – 40 mph

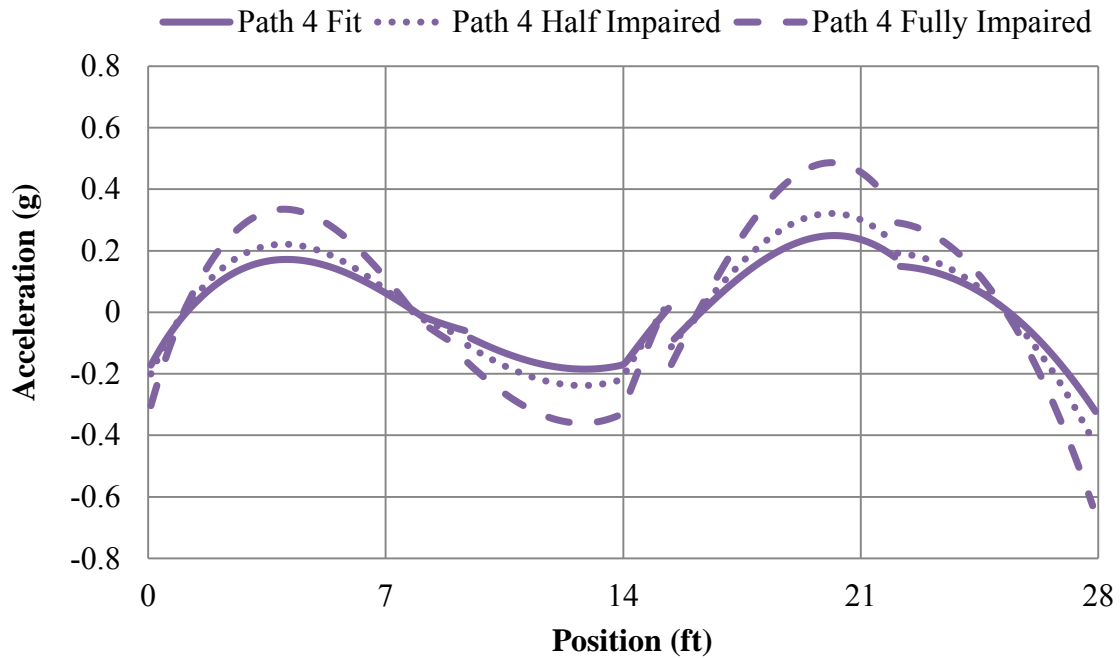


Fig. 3.8. Path 4 MATLAB wheel path accelerations – 40 mph

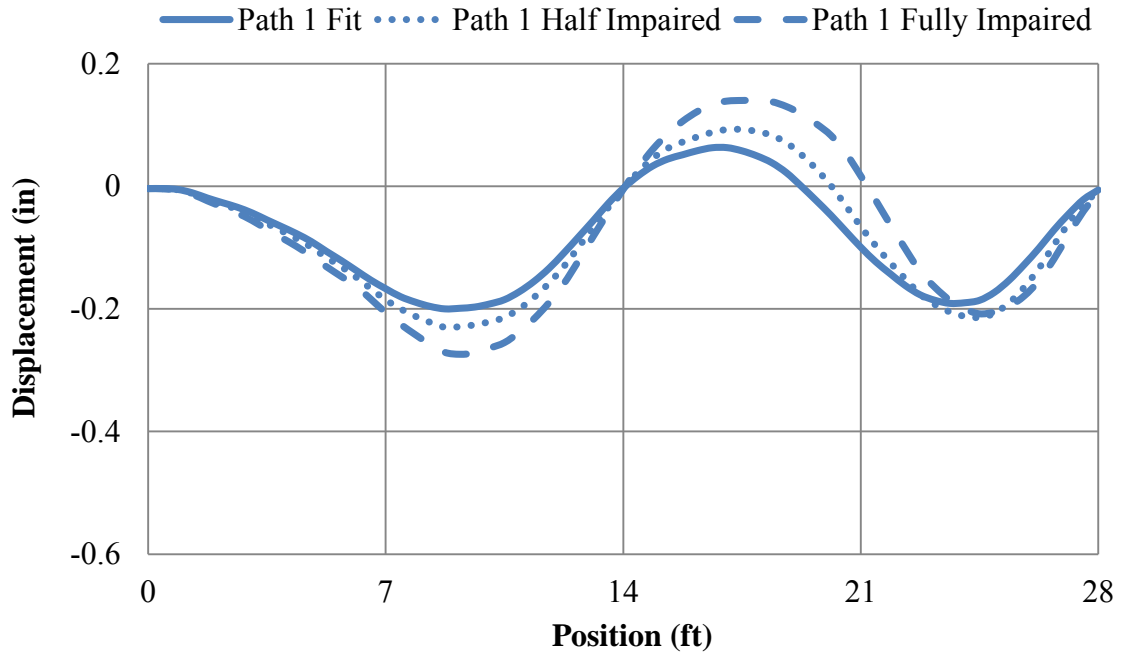


Fig. 3.9. Path 1 LS-DYNA wheel path displacements – 40 mph

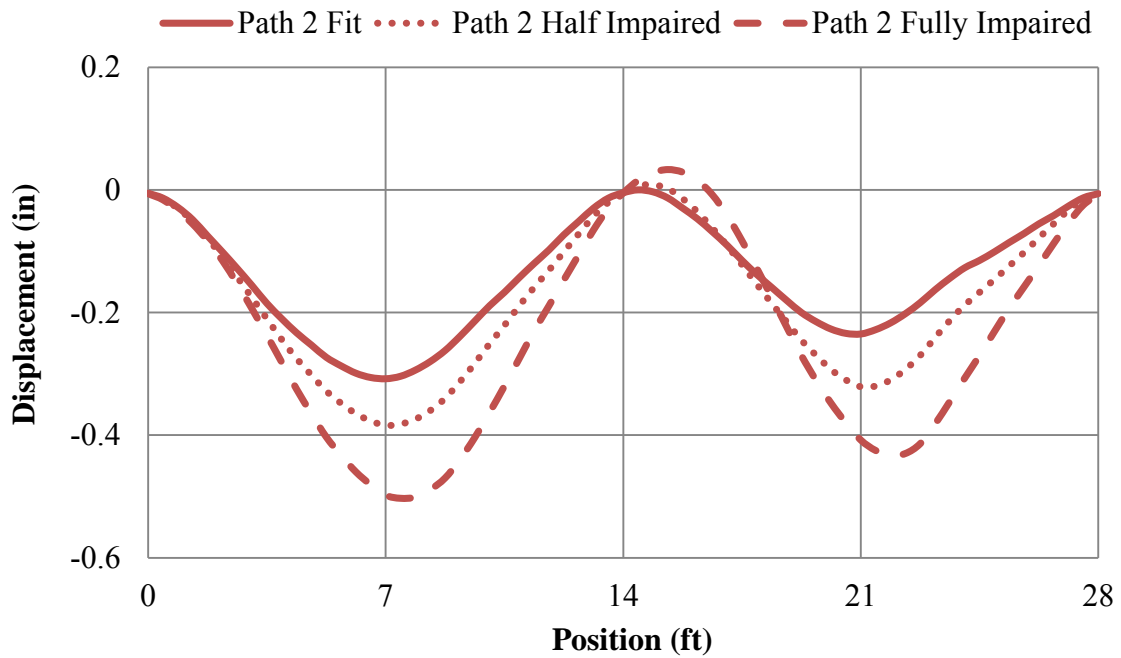


Fig. 3.10. Path 2 LS-DYNA wheel path displacements – 40 mph

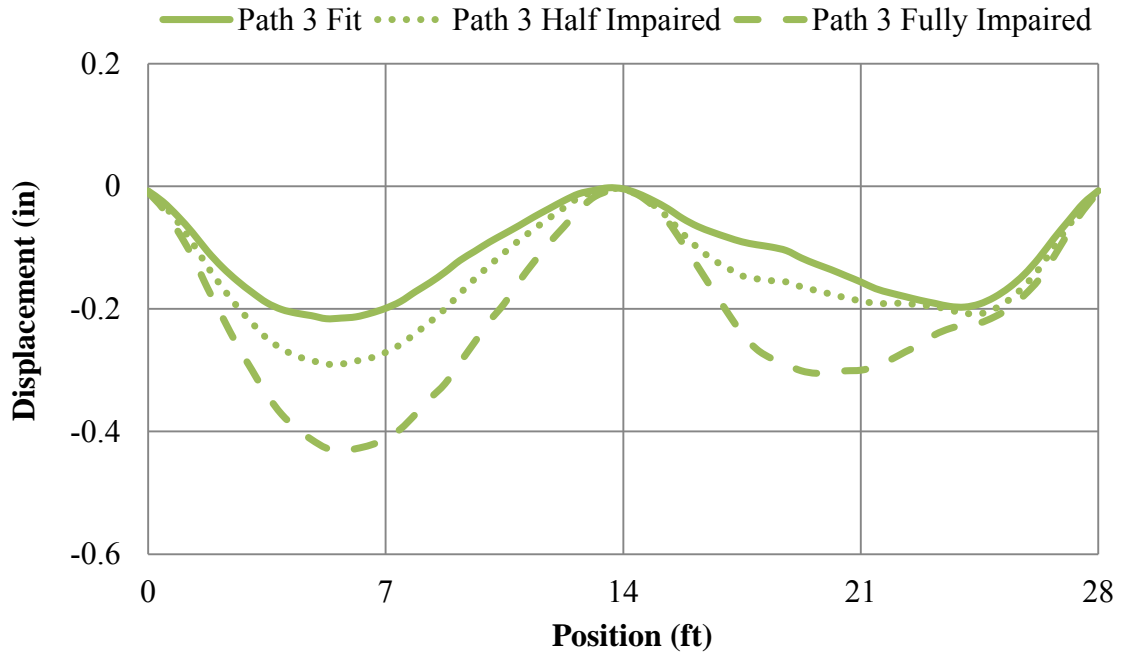


Fig. 3.11. Path 3 LS-DYNA wheel path displacements – 40 mph

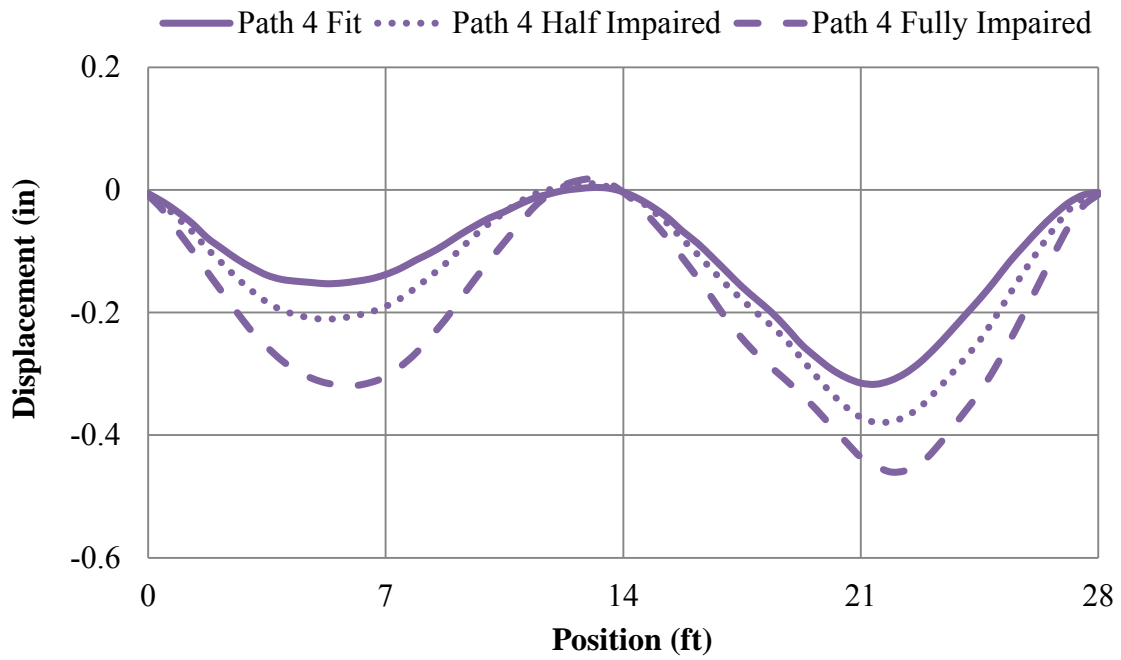


Fig. 3.12. Path 4 LS-DYNA wheel path displacements – 40 mph

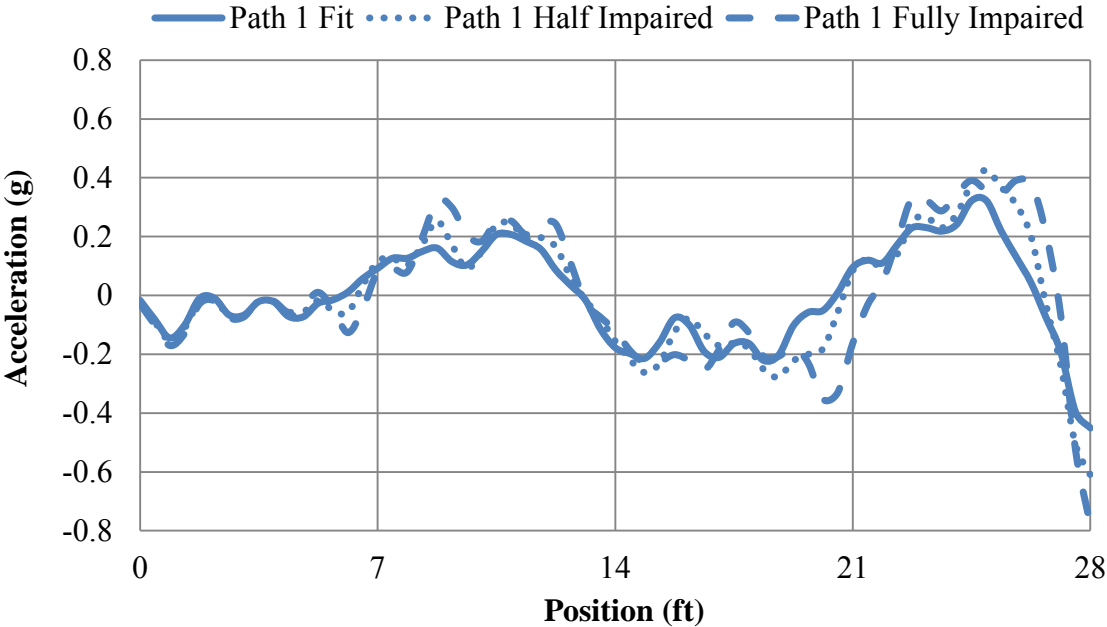


Fig. 3.13. Path 1 LS-DYNA wheel path accelerations – 40 mph

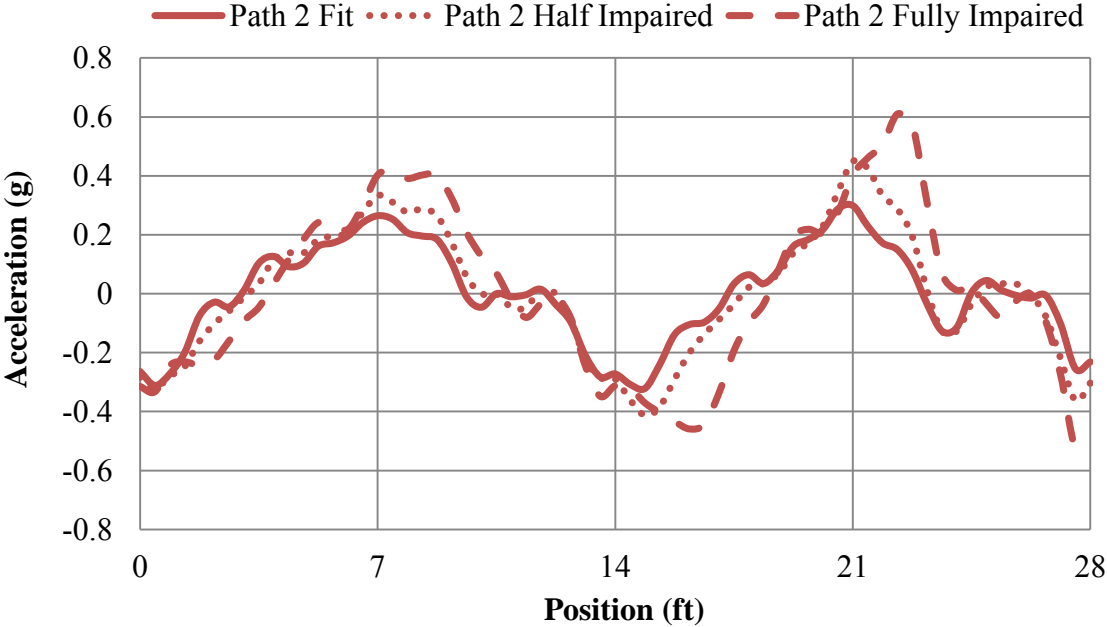


Fig. 3.14. Path 2 LS-DYNA wheel path accelerations – 40 mph

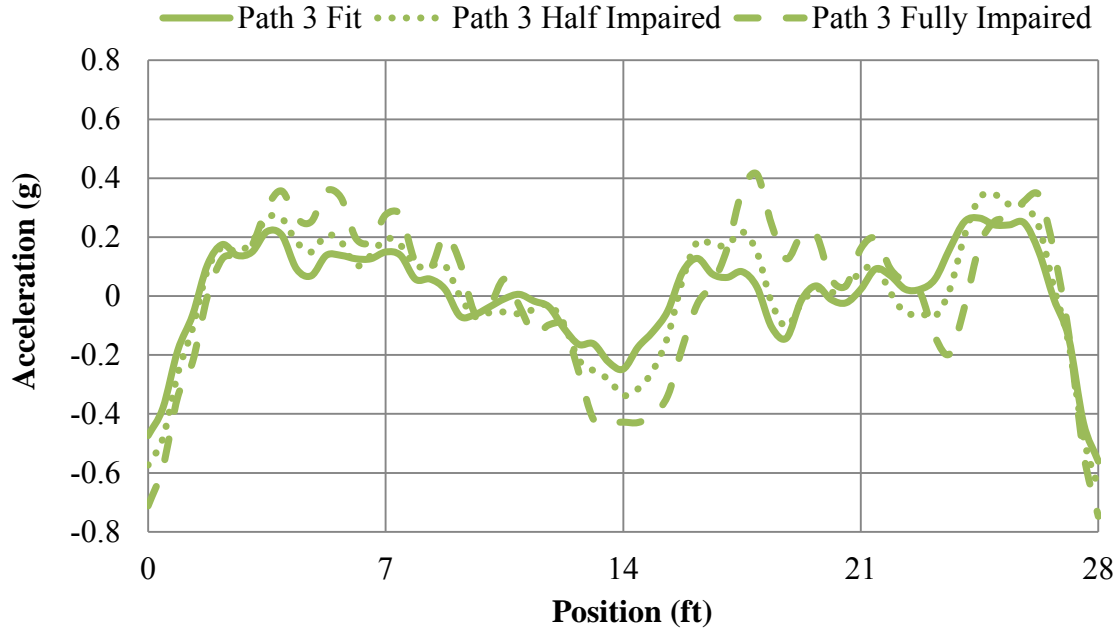


Fig 3.15. Path 3 LS-DYNA wheel path accelerations – 40 mph

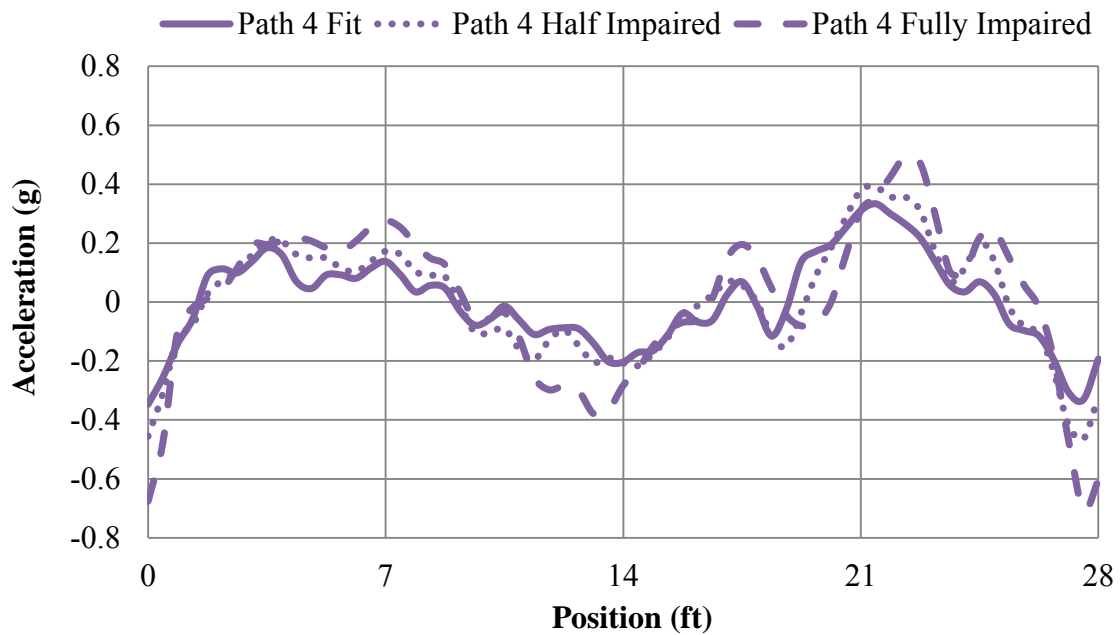


Fig. 3.16. Path 4 LS-DYNA wheel path accelerations – 40 mph

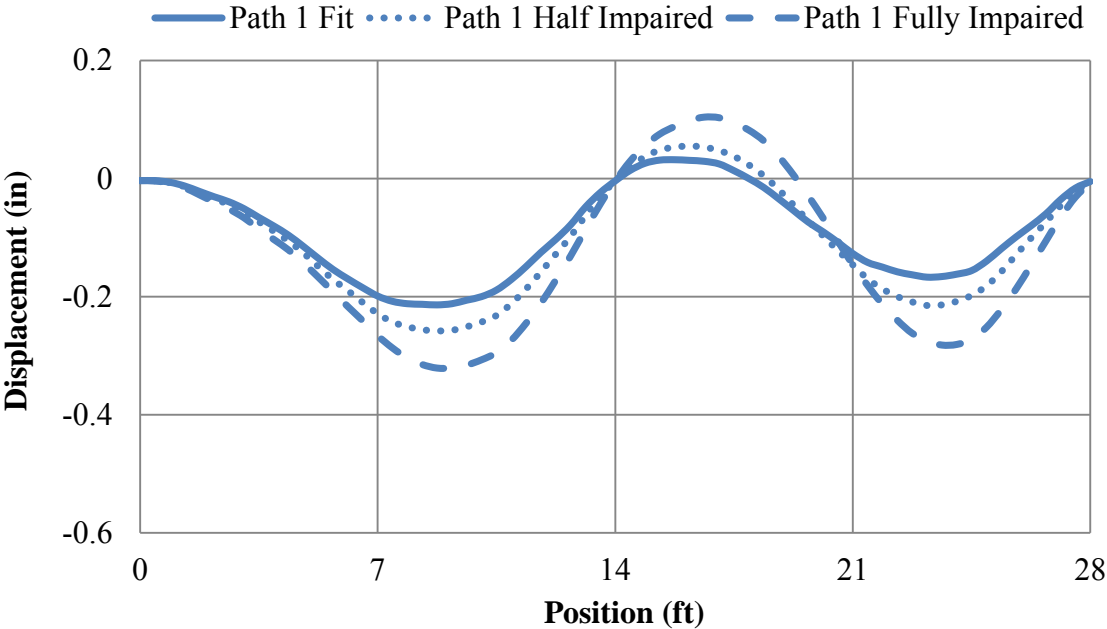


Fig. 3.17. Path 1 LS-DYNA wheel path displacements – 30 mph

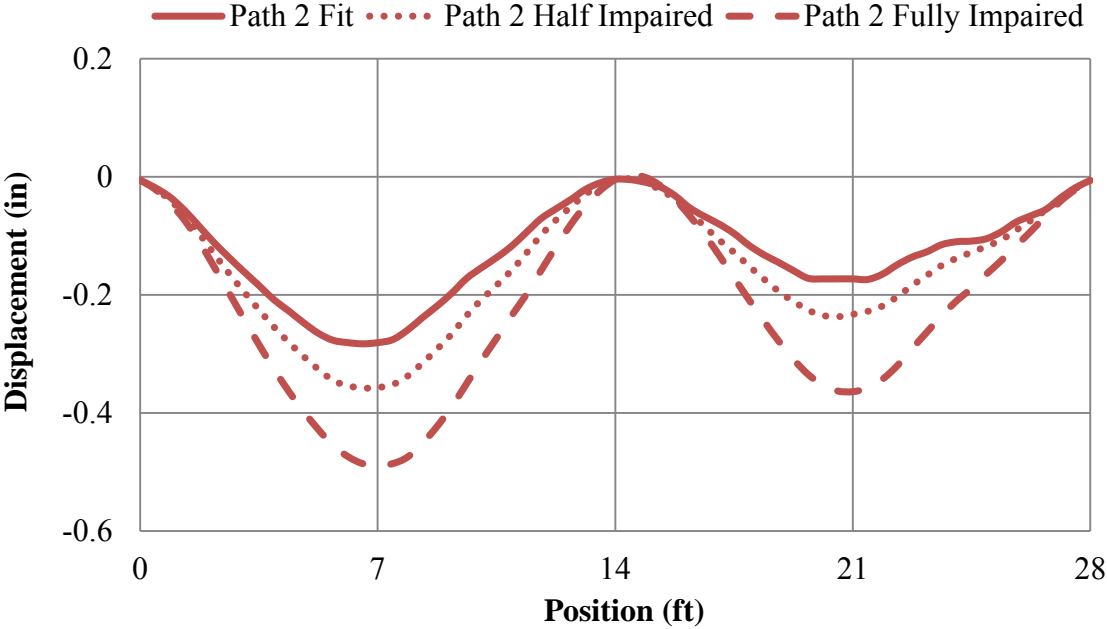


Fig. 3.18. Path 2 LS-DYNA wheel path displacements – 30 mph

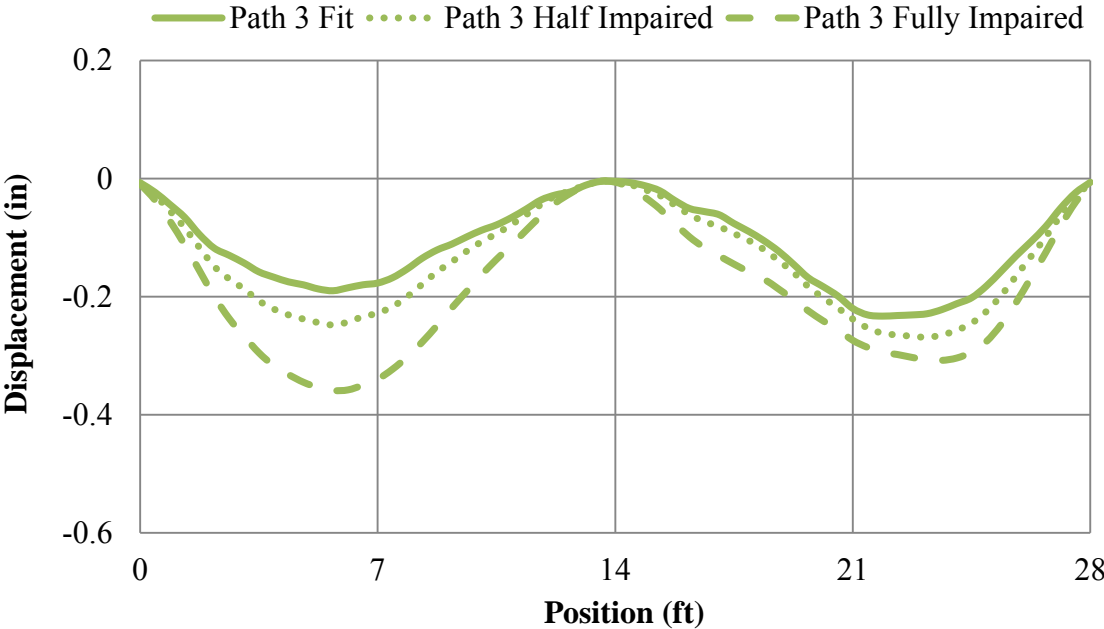


Fig. 3.19. Path 3 LS-DYNA wheel path displacements – 30 mph

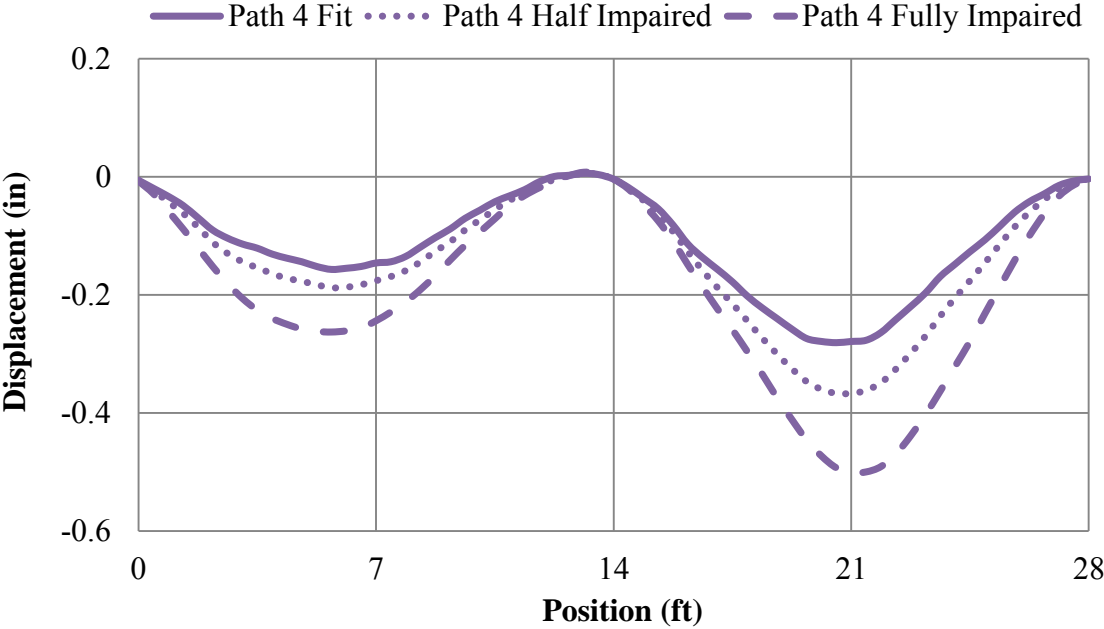


Fig. 3.20. Path 4 LS-DYNA wheel path displacements – 30 mph

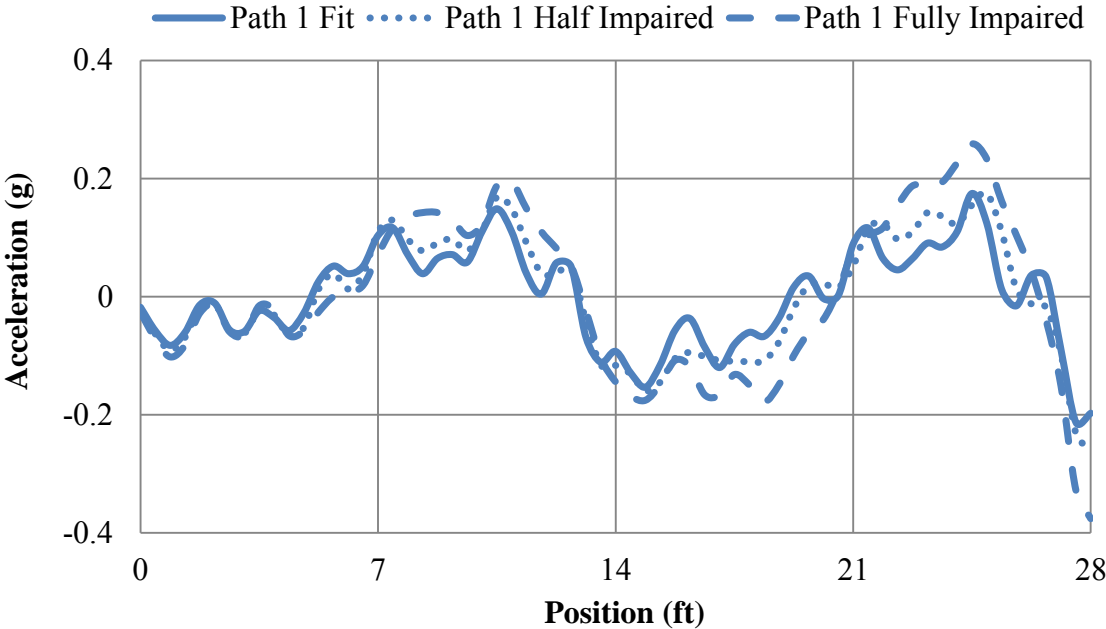


Fig 3.21. Path 1 wheel path accelerations – 30 mph

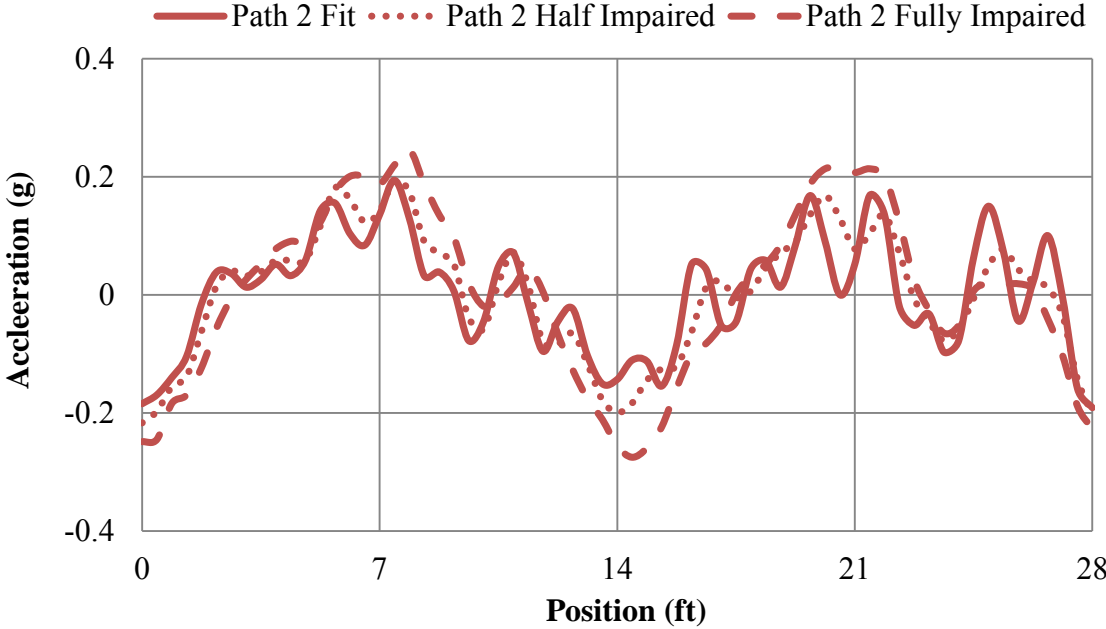


Fig. 3.22. Path 2 wheel path accelerations – 30 mph

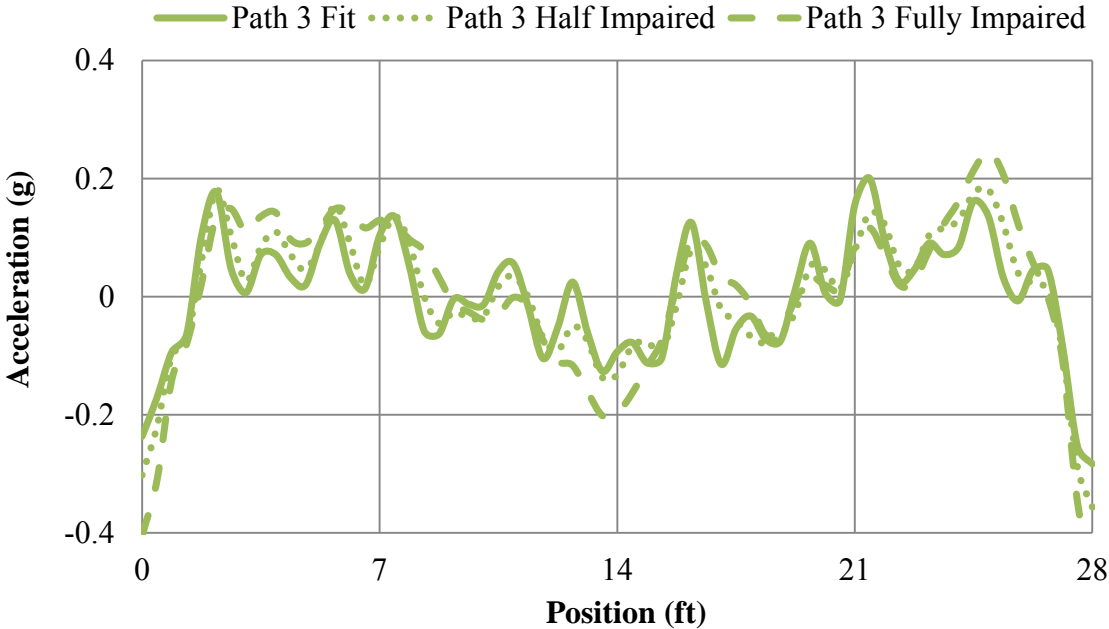


Fig. 3.23. Path 3 wheel path accelerations – 30 mph

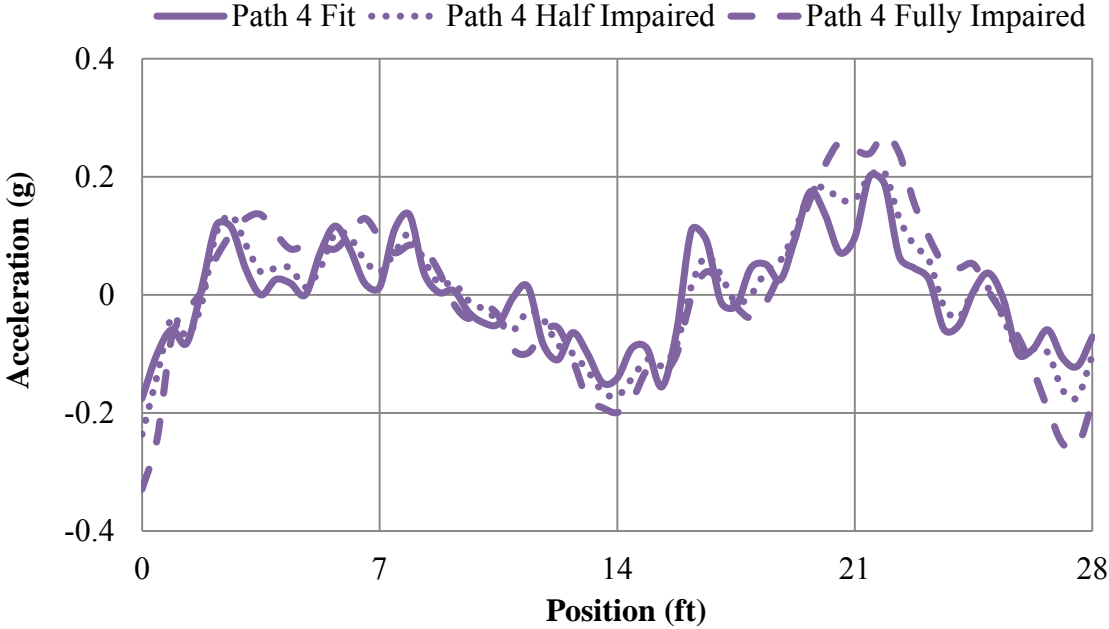


Fig. 3.24. Path 4 wheel path accelerations – 30 mph

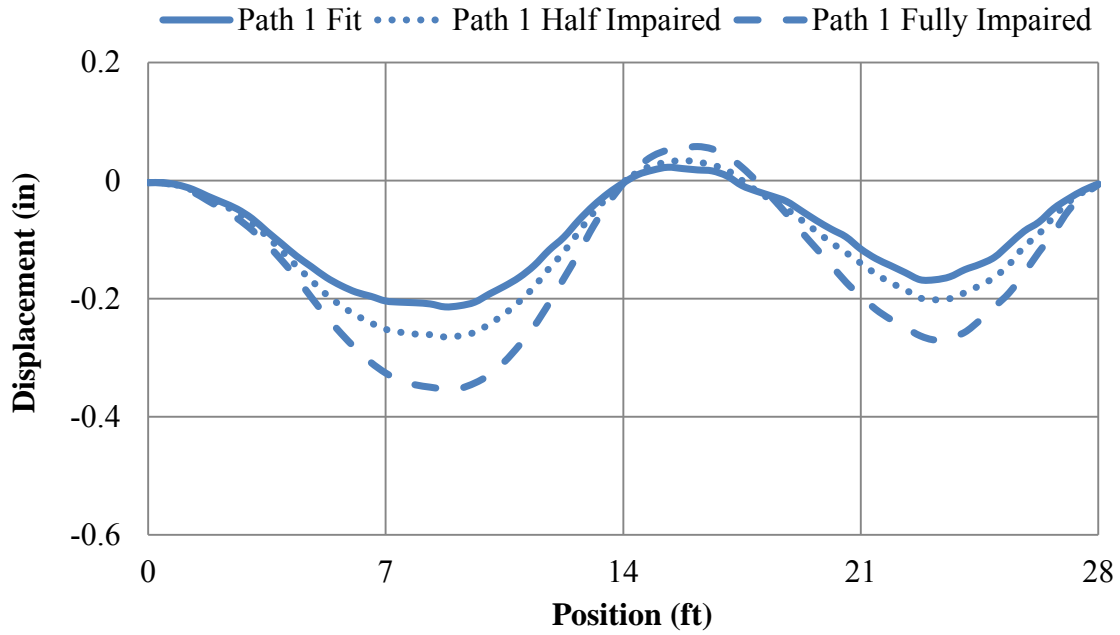


Fig 3.25. Path 1 LS-DYNA wheel path displacements – 20 mph

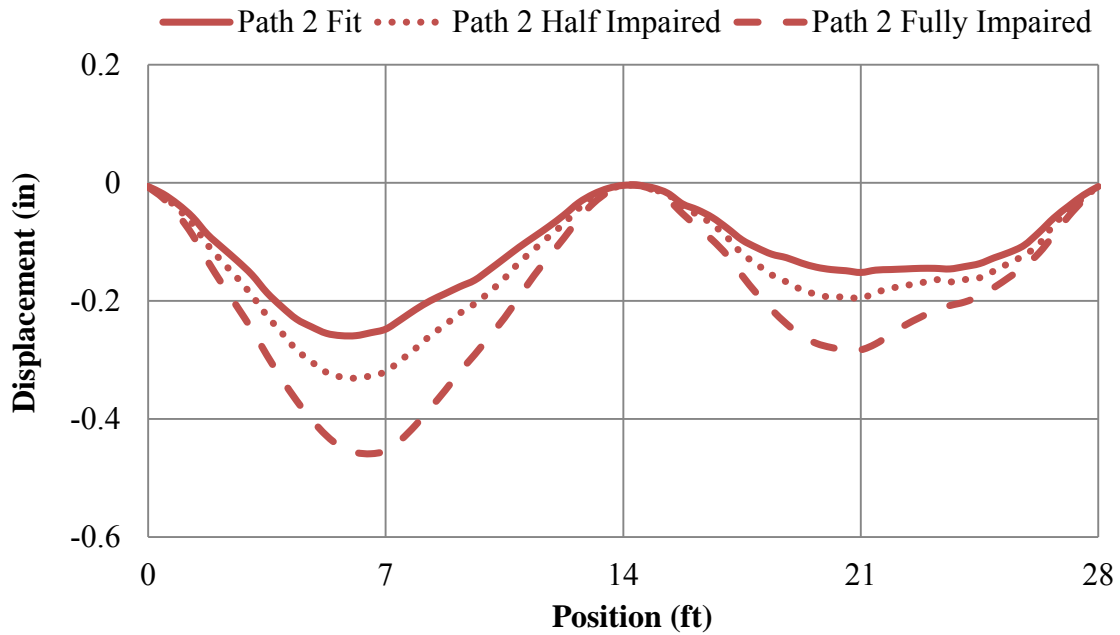


Fig. 3.26. Path 2 LS-DYNA wheel path displacements – 20 mph

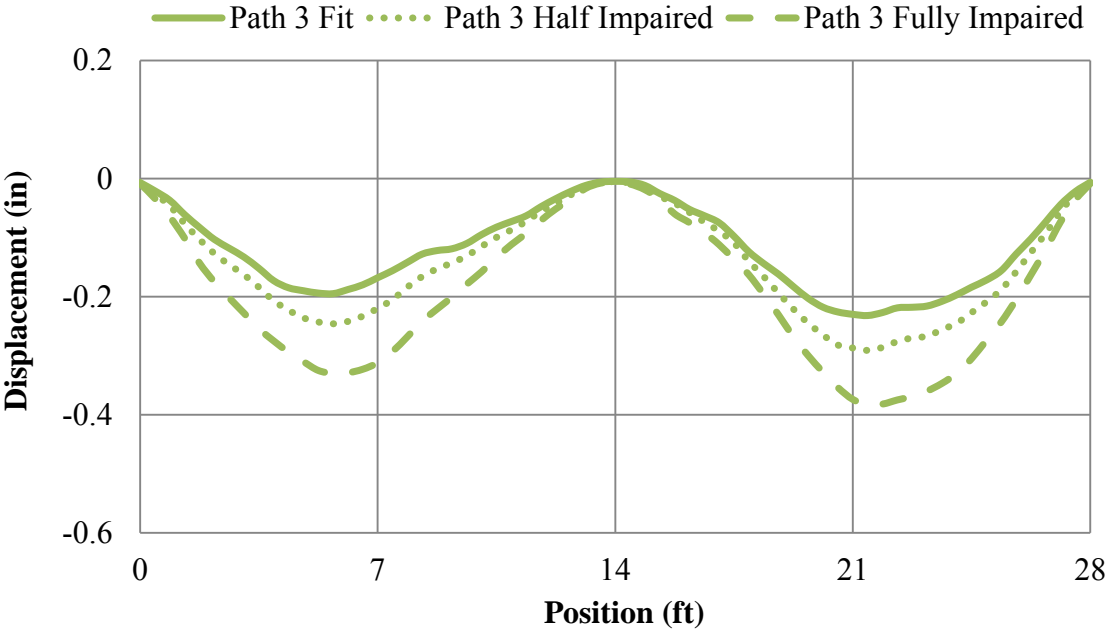


Fig. 3.27. Path 3 LS-DYNA wheel path displacements – 20 mph

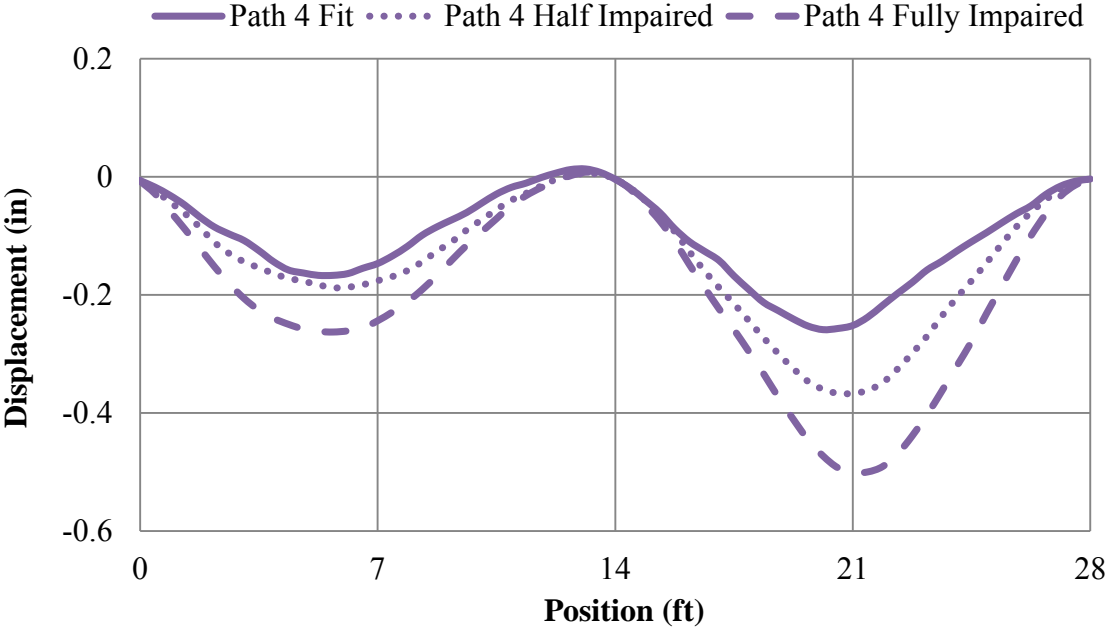


Fig 3.28. Path 4 LS-DYNA wheel path displacements – 20 mph

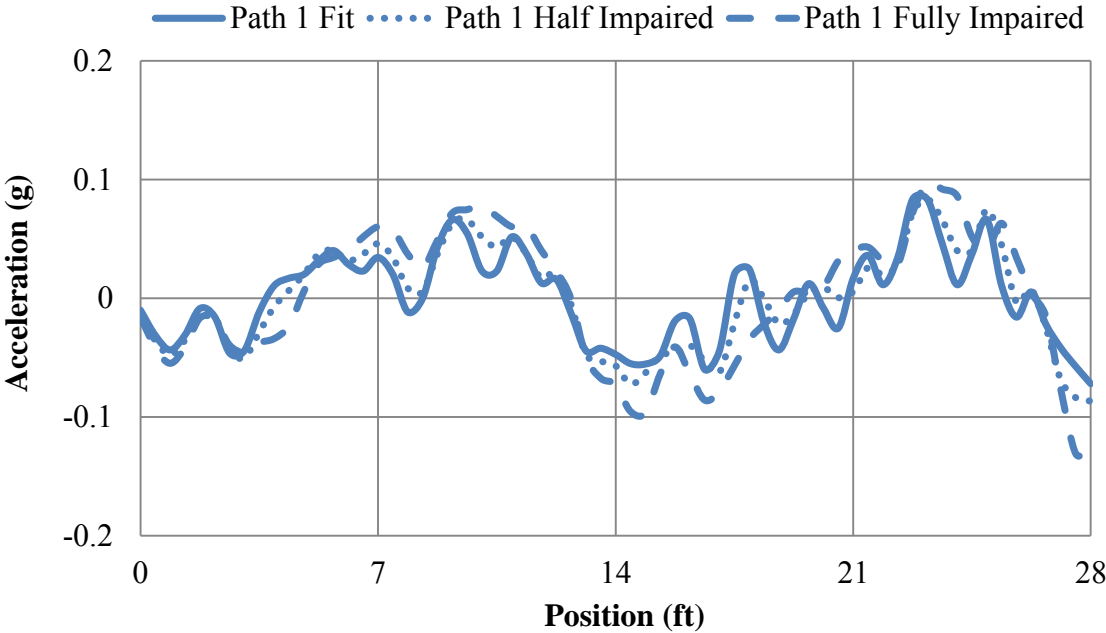


Fig. 3.29. Path 1 LS-DYNA wheel path accelerations – 20 mph

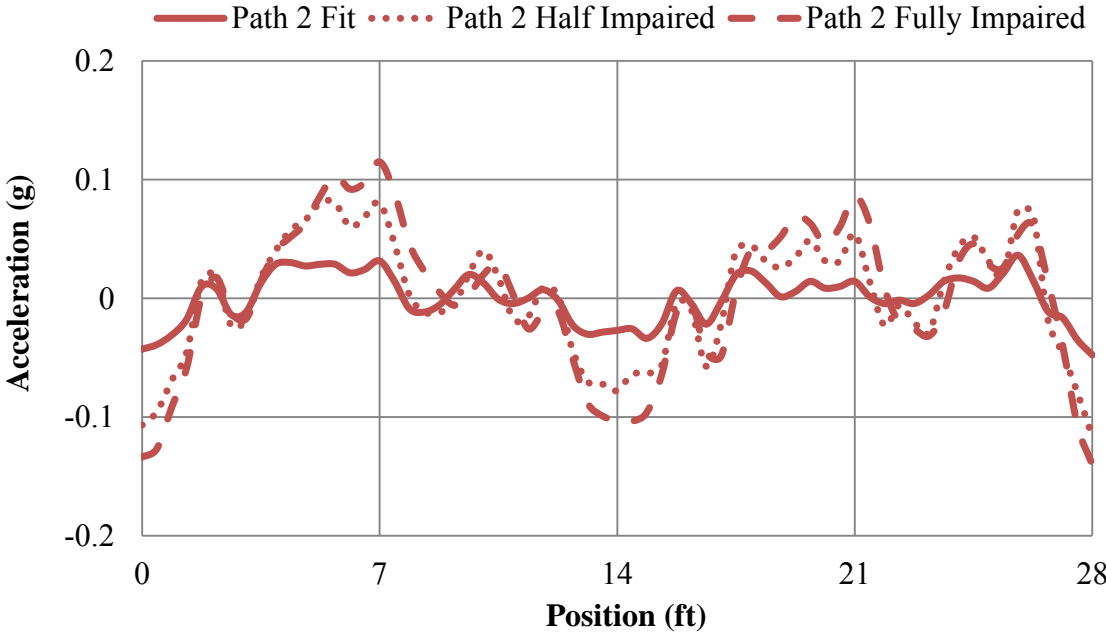


Fig. 3.30. Path 2 LS-DYNA wheel path accelerations – 20 mph

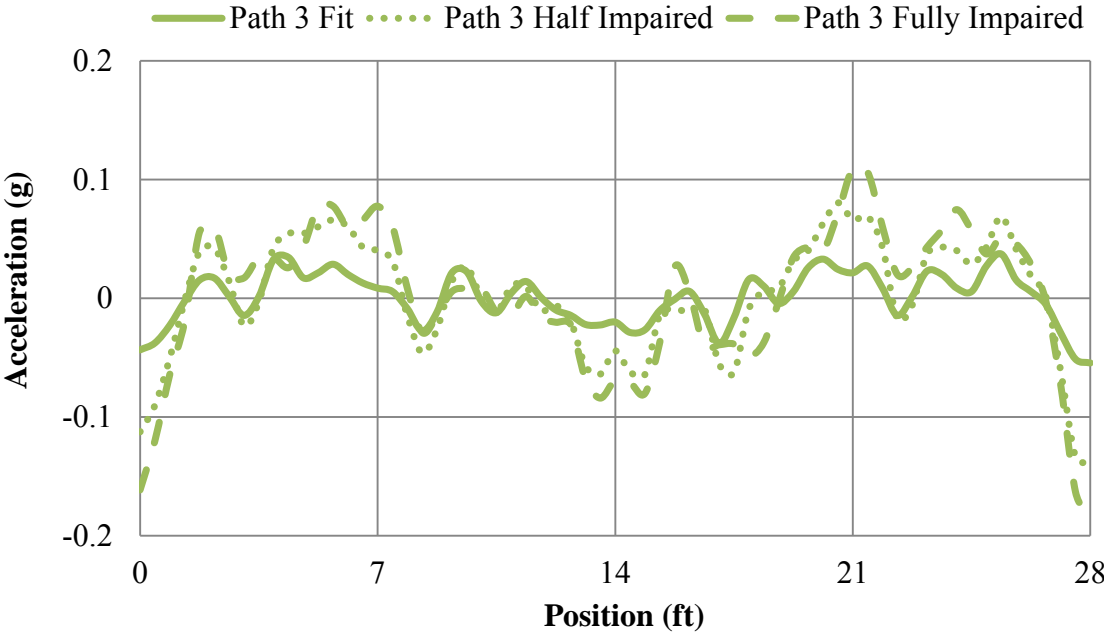


Fig. 3.31. Path 3 LS-DYNA wheel path accelerations – 20 mph

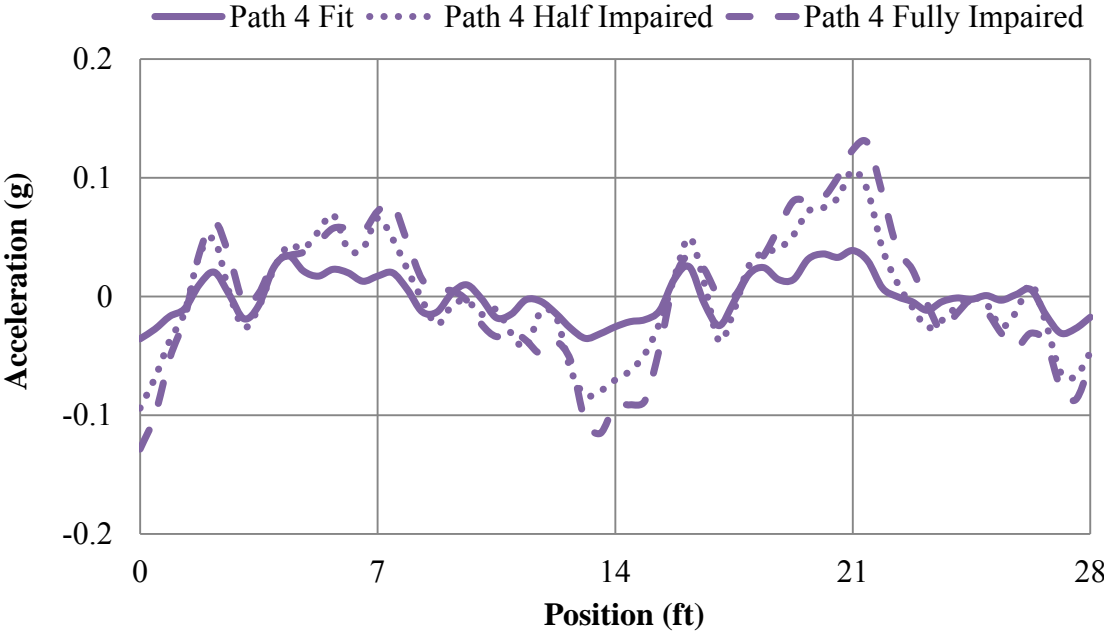


Fig. 3.32. Path 4 LS-DYNA wheel path accelerations – 20 mph

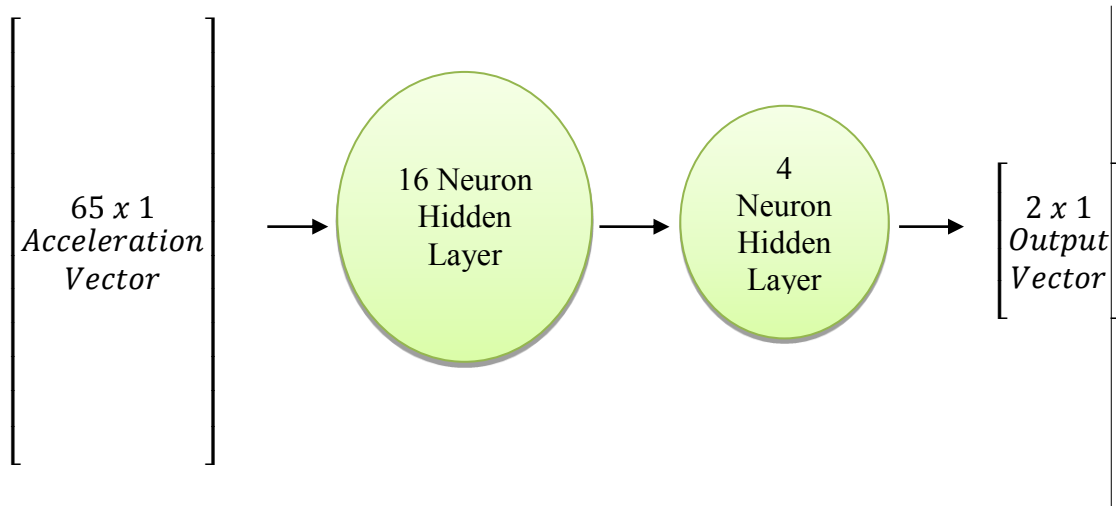


Fig. 4.1. Network architecture

$\begin{bmatrix} 1 \\ 0 \end{bmatrix}$: *Fit*

$\begin{bmatrix} 1 \\ 1 \end{bmatrix}$: *Half Impaired*

$\begin{bmatrix} 0 \\ 1 \end{bmatrix}$: *Fully Impaired*

Fig. 4.2. Output vector options

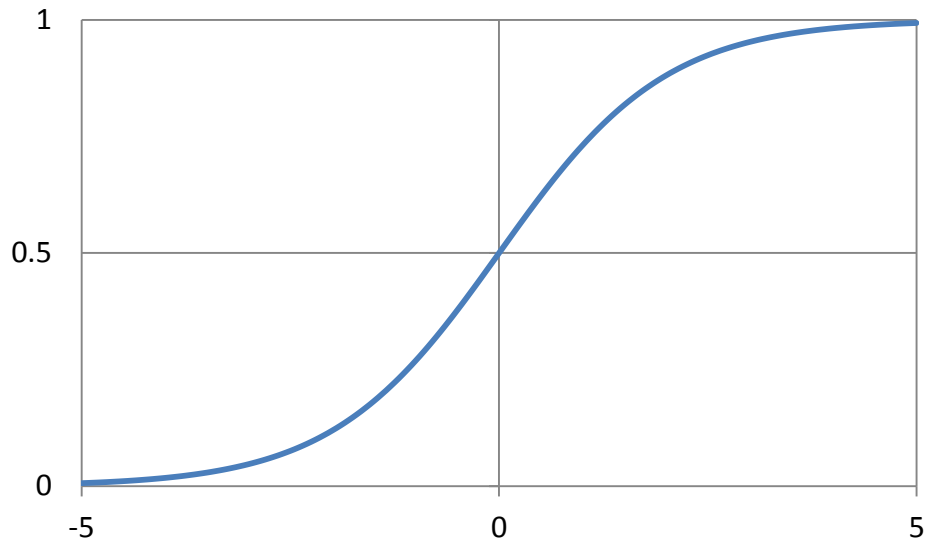


Fig. 4.3. Logsig function

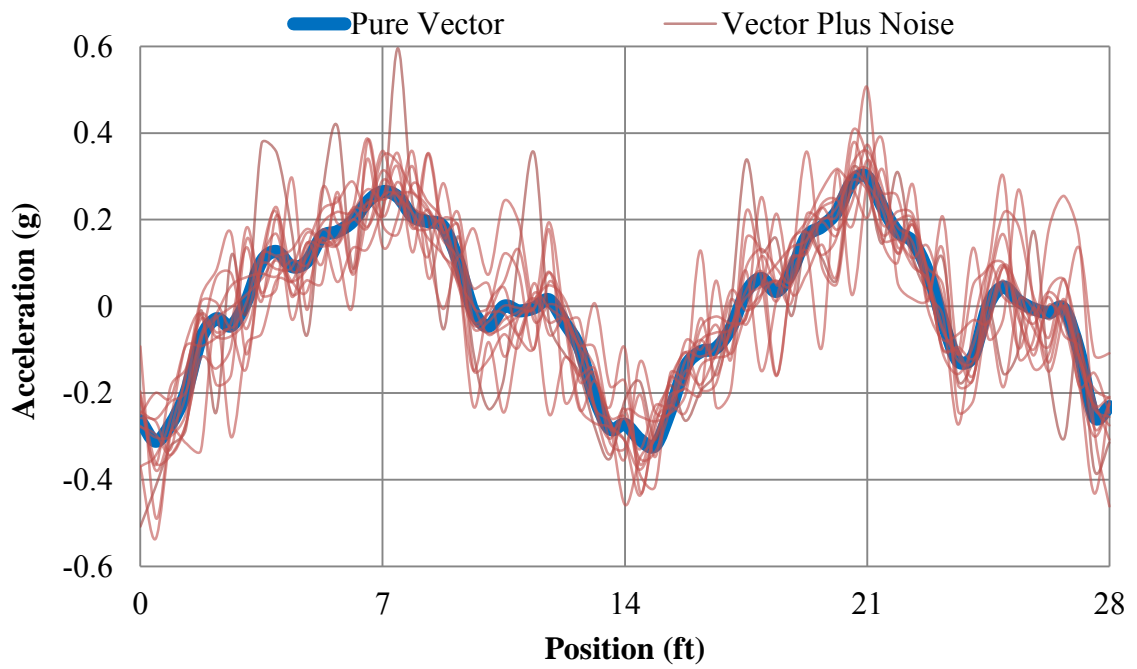


Fig. 4.4. Acceleration vector with noise added

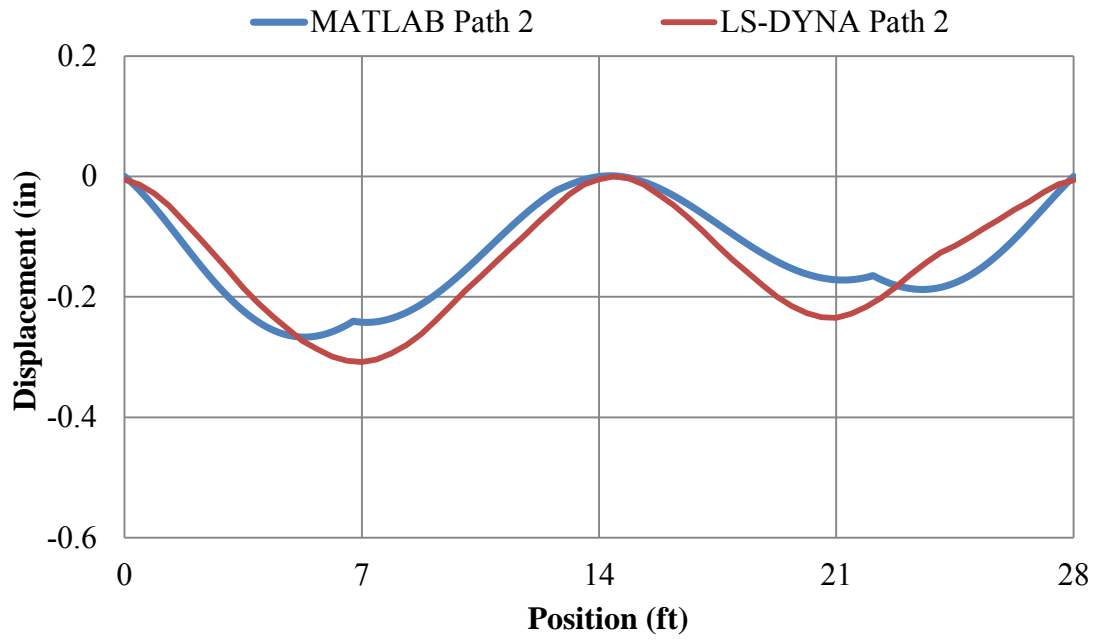


Fig. 6.1. Comparison between displacements from MATLAB and LS-DYNA path 2

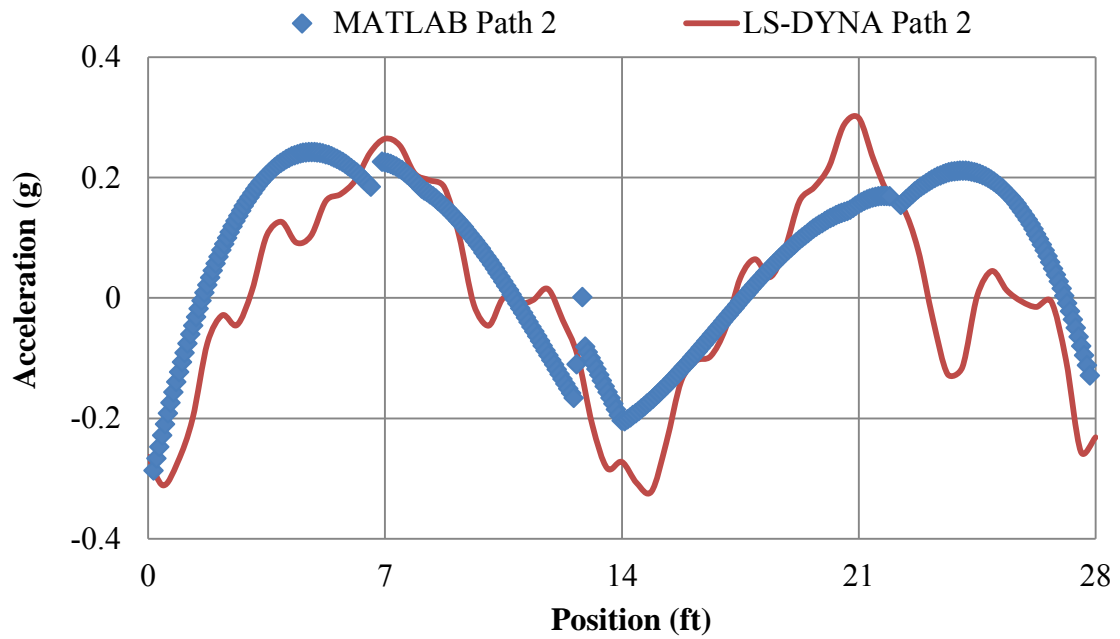


Fig 6.2. Comparisons between accelerations from MATLAB and LS-DYNA path 2

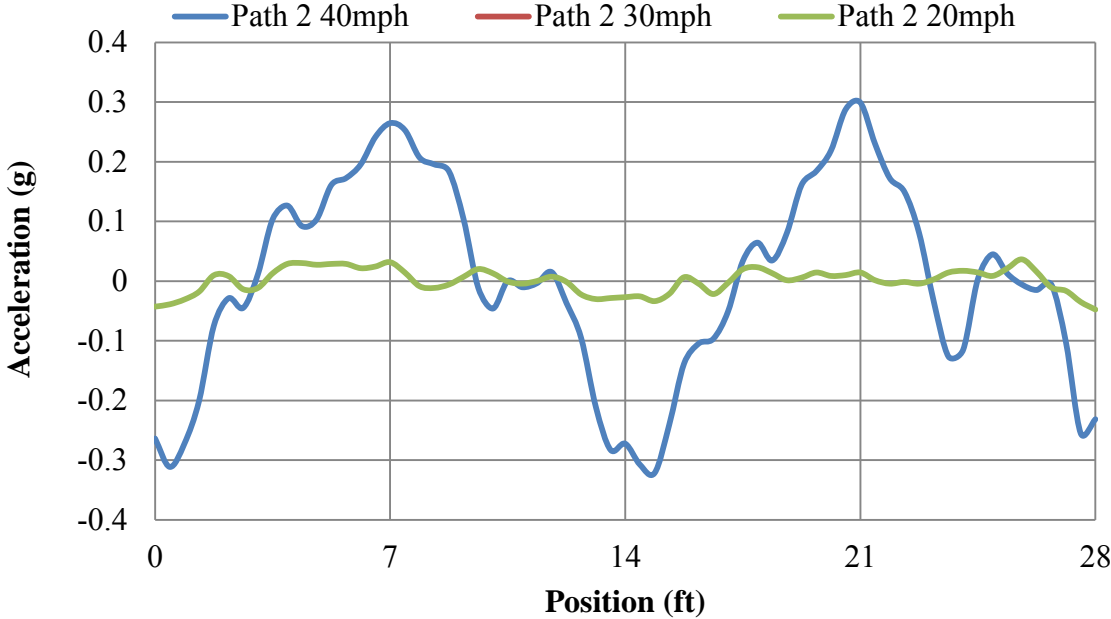


Fig 6.3. Comparisons between accelerations at different train speeds

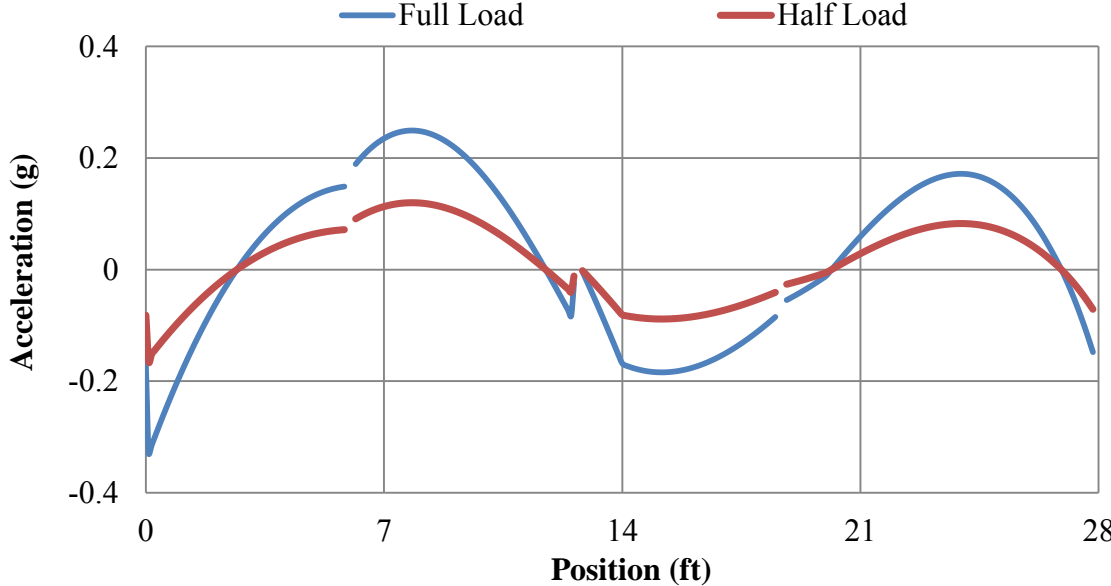


Fig 6.4. Comparisons between accelerations under different load conditions

APPENDIX B
TABLES

Table 1.1. Summary of previous testing

Specimen	Intact EI Value (k-in²)	Split EI Value (k-in²)	% Reduction
2F	2856700	1073700	62.4
17F	3140200	1168100	62.8
Average	2998450	1120900	62.6

Table 2.1. General bridge parameters

Parameter	Description
# of Spans	2
Span Length	14 ft
Stringers per Chord	4
Load	Freight Car Connection
Axle Load Value	78.75 kips
Axle Spacing	Standard

Table 2.2. Material properties

Material	EI Intact (kip-in²)	EI Split (kip-in²)	ρ (lbf-sec²/in⁴)
Southern Pine Stringer	2,998,450	1,120,900	7.76×10^{-5}
136 lbs/yd Rail	2,827,200	N/A	7.32×10^{-4}
Cross Tie	339,570	N/A	7.76×10^{-5}

Table 5.1. Percentage of correct outputs - MATLAB input, 40 mph train speed

	Bridge Condition			Avg.
	Fit %	Half %	Full %	
Path 1	93	60	100	84
Path 2	100	90	100	97
Path 3	100	70	100	90
Path 4	87	70	100	86
A.C. Correct	100	70	100	90
A.C. Incorrect	0	7	0	2
No Decision	0	23	0	8

Table 5.2. Percentage of correct outputs - MATLAB input, 30 mph train speed

	Bridge Condition			Avg
	Fit	Half	Full	
Path 1	93	70	85	83
Path 2	70	45	100	72
Path 3	80	60	95	78
Path 4	85	50	100	78
A.C. Correct	83	53	100	79
A.C. Incorrect	0	13	0	4
No Decision	17	44	0	17

Table 5.3. Percentage of correct outputs – LS-DYNA input, 40 mph train speed

	Bridge Condition			Avg
	Fit	Half	Full	
Path 1	100	97	97	98
Path 2	100	87	97	94
Path 3	100	97	93	97
Path 4	100	100	97	99
A.C. Correct	100	97	100	99
A.C. Incorrect	0	0	0	0
No Decision	0	3	0	1

Table 5.4. Percentage of correct outputs – LS-DYNA input, 30 mph train speed

	Bridge Condition			Avg
	Fit	Half	Full	
Path 1	87	70	95	84
Path 2	85	80	100	88
Path 3	95	95	90	93
Path 4	85	60	80	75
A.C. Correct	97	80	97	91
A.C. Incorrect	0	3	0	1
No Decision	3	17	3	8

Table 5.5. Percentage of correct outputs - combined input, 40 mph train speed

	Bridge Condition			Avg
	Fit	Half	Full	
Path 1	90	73	80	81
Path 2	97	90	100	96
Path 3	97	83	97	92
Path 4	97	53	100	83
A.C. Correct	100	73	97	90
A.C. Incorrect	0	3	0	1
No Decision	0	14	3	8

Table 5.6. Percentage of correct outputs - combined input, 30 mph train speed

	Bridge Condition			Avg
	Fit	Half	Full	
Path 1	100	40	60	67
Path 2	100	20	100	73
Path 3	80	60	100	80
Path 4	80	70	60	70
A.C. Correct	100	30	80	70
A.C. Incorrect	0	20	0	7
No Decision	0	50	20	23

APPENDIX C

CODE FOR MATLAB MODEL

```

%%This file calculates the wheel path displacements for a two span
%timber bridge. Each span has a length of 14'. Therefore, based on
%typical wheel spacings only 5 wheel loads will be on the bridge at
%once. This relates to 4 total spacings.

%Define spacing matrix in inches
%a=[a1 a2 a3 a4...ai]
spaces=[6*12 6.67*12 6*12 0];
a=round(spaces);

%Define load matrix in lbs
%P=[P1 P2 P3 P4 P5...Pi]
P=[78750 78750 78750 78750 0 ];

%Input Constants
syms s; %distance from left support to load
L=28*12; %length of one span, in
Ir=2*94.24 %moment of inertia of rail, in^4
Er=30*10^6 %Young's modulus of rail, psi
EIr=2*(94.24)*30*10^6; %Combined rigidity of two rails, lb-in^2
EIs=2059675*8000; %Combined rigidity of eight stringers

%Input equations
thetar = s/(48*EIr*L)*(7*L^2-24*L*s+20*s^2);
thetas = s/(48*EIs*L)*(7*L^2-24*L*s+20*s^2);
Vo = 1 - (5*s)/(2*L) + (2*s^3)/(L^3);
Rb = s/(L^3)*(3*L^2-4*s^2);
Rb = s/(L^3)*(3*L^2-4*s^2);

%Preallocate for speed
y1r=zeros(L+sum(a),336);
y1s=y1r;y2r=y1r;y2s=y1r;y3r=y1r;y3s=y1r;y4r=y1r;y4s=y1r;y5r=y1r;y5s=y1;
Y1=zeros(L+sum(a),336);
Y2=Y1;Y3=Y1;Y4=Y1;Y5=Y1;

%Calculate deflections based on unit load P and a matrices. Individual
%deflections due to individual wheels will be referred to as yi.
for s=1:L
    i=s;
    for x=1:(L-1)
        j=x;
        %y1 are deflections for load 1
        if x<=s & s<=L/2
            y1r(i,j)=subs(thetar,s)*x - (subs(Vo,s)*x^3)/(6*EIr);
            y1s(i,j)=subs(thetas,s)*x - (subs(Vo,s)*x^3)/(6*EIs);
        elseif s<=x & x<=L/2
            y1r(i,j)=subs(thetar,s)*x - (subs(Vo,s)*x^3)/(6*EIr) + (x-
s)^3/(6*EIr);

```

```

        y1s(i,j)=subs(thetas,s)*x - (subs(Vo,s)*x^3)/(6*EIs) + (x-
        s)^3/(6*EIs);
elseif s<=L/2 & x>=L/2
    y1r(i,j)=subs(thetar,s)*x - (subs(Vo,s)*x^3)/(6*EIr) + (x-
    s)^3/(6*EIr) - (subs(Rb,s)*(x-L/2)^3)/(6*EIr);
    y1s(i,j)=subs(thetas,s)*x - (subs(Vo,s)*x^3)/(6*EIs) + (x-
    s)^3/(6*EIs) - (subs(Rb,s)*(x-L/2)^3)/(6*EIs);
end
%Impose symmetry
if s>L/2 & s<L
    y1r(L-i+L/2,j)=y1r(i-L/2,L-j);
    y1s(L-i+L/2,j)=y1s(i-L/2,L-j);
end
end
end

%y1 represents unit deflections for a point load. These can be used for
%all wheels spaced accordingly.
for k=1:L-1
    y2r(k+a(1),:)=y1r(k,:);
    y2s(k+a(1),:)=y1s(k,:);
    y3r(k+a(1)+a(2),:)=y1r(k,:);
    y3s(k+a(1)+a(2),:)=y1s(k,:);
    y4r(k+a(1)+a(2)+a(3),:)=y1r(k,:);
    y4s(k+a(1)+a(2)+a(3),:)=y1s(k,:);
    y5r(k+sum(a),:)=y1r(k,:);
    y5s(k+sum(a),:)=y1s(k,:);
end

%Equation derived for deflection based on known quantities. Equation is
%deflection=(load*yr*ys)/(yr+ys)
Y1=P(1)*(y1r.*y1s)./(y1r+y1s);
Y2=P(2)*(y2r.*y2s)./(y2r+y2s);
Y3=P(3)*(y3r.*y3s)./(y3r+y3s);
Y4=P(4)*(y4r.*y4s)./(y4r+y4s);
Y5=P(5)*(y5r.*y5s)./(y5r+y5s);

%Force zeros
Y1(L:L+sum(a),:)=0; Y1(14*12,:)=0;
Y2(1:a(1),:)=0; Y2(L+a(1):L+sum(a),:)=0; Y2(a(1)+168,:)=0;
Y3(1:(a(1)+a(2)),:)=0; Y3(L+a(1)+a(2):L+sum(a),:)=0;
Y3(a(1)+a(2)+168,:)=0;
Y4(1:(a(1)+a(2)+a(3)),:)=0; Y4(L+a(1)+a(2)+a(3):L+sum(a),:)=0;
Y4(a(1)+a(2)+a(3)+168,:)=0;
Y5(1:sum(a),:)=0; Y5(sum(a)+168,:)=0;

%Add deflections together to get one deflection matrix
Y=Y1+Y2+Y3+Y4+Y5;
Y(:,14*12)=0;

```

VITA

Name: John Paul Orsak

Address: Association of American Railroads Affiliated Laboratory
Texas Transportation Institute
Texas A&M University System
3135 TAMU
College Station, TX 77843-3135

Email Address: john.orsak@gmail.com

Education: B.S., Civil Engineering, Texas A&M University, 2010
M.S., Civil Engineering, Texas A&M University, 2012